Perfecting Our Set of Spectrophotometric Standard DA White Dwarfs

Annalisa Calamida[1] ◉, Thomas Matheson[2] ◉, Edward W. Olszewski[3] ◉, Abhijit Saha[2] ◉, Tim Axelrod[3] ◉, Clare Shanahan[1],
Jay Holberg[4], Sean Points[5] ◉, Gautham Narayan[6,7] ◉, Konstantin Malanchev[6,8] ◉, Ryan Ridden-Harper[9] ◉,
Nicola Gentile-Fusillo[10] ◉, Roberto Raddi[11] ◉, Ralph Bohlin[1] ◉, Armin Rest[1,12] ◉, Ivan Hubeny[3] ◉, Susana Deustua[13,15] ◉,
John Mackenty[1], Elena Sabbi[1] ◉, and Christopher W. Stubbs[14] ◉

[1] Space Telescope Science Institute—AURA, 3700 San Martin Dr., Baltimore, MD 21218, USA; calamida@stsci.edu
[2] NSF's National Optical-Infrared Astronomy Research Laboratory, 950 N Cherry Ave., Tucson, AZ 85749, USA
[3] Steward Observatory, The University of Arizona, 933 N Cherry Ave, Tucson, AZ 85719, USA
[4] Lunar and Planetary Laboratory, The University of Arizona, 1629 E University Blvd., Tucson, AZ 85721, USA
[5] Cerro Tololo Inter-American Observatory, Casilla 603, La Serena, Chile
[6] University of Illinois Urbana-Champaign, 1002 W Green St. M/C 221 Urbana, IL 61801, USA
[7] Center for AstroPhysical Surveys, National Center for Supercomputing Applications, 1205 W Clark St., Urbana, IL 61801, USA
[8] Sternberg Astronomical Institute, Lomonosov Moscow State University, Universitetsky pr. 13, Moscow 119234, Russia
[9] University of Canterbury, 20 Kirkwood Ave., Upper Riccarton, 8041 Christchurch, New Zealand
[10] European Southern Observatory, Karl Schwarzschild Straße 2, D-85748 Garching, Germany
[11] Universitat Politècnica de Catalunya, Departament de Física, c/ Esteve Terrades 5, E-08860 Castelldefels, Spain
[12] Department of Physics and Astronomy, Johns Hopkins University, Baltimore, MD 21218, USA
[13] Sensor Science Division, National Institute of Standards and Technology, 100 Bureau Dr., MS 8444, Gaithersburg, MD 20899, USA
[14] Department of Physics, Department of Astronomy, Harvard University, 17 Oxford St. Cambridge, MA 02138, USA

Abstract

We verified for photometric stability a set of DA white dwarfs with Hubble Space Telescope magnitudes from the near-ultraviolet to the near-infrared and ground-based spectroscopy by using time-spaced observations from the Las Cumbres Observatory network of telescopes. The initial list of 38 stars was whittled to 32 final ones, which comprise a high-quality set of spectrophotometric standards. These stars are homogeneously distributed around the sky and are all fainter than $r \sim 16.5$ mag. Their distribution is such that at least two of them would be available to be observed from any observatory on the ground at any time at airmass less than 2. Light curves and different variability indices from the Las Cumbres Observatory data were used to determine the stability of the candidate standards. When available, Pan-STARRS1, Zwicky Transient Facility, and TESS data were also used to confirm the star classification. Our analysis showed that four DA white dwarfs may exhibit evidence of photometric variability, while a fifth is cooler than our established lower temperature limit, and a sixth star might be a binary. In some instances, due to the presence of faint nearby red sources, care should be used when observing a few of the spectrophotometric standards with ground-based telescopes. Light curves and finding charts for all the stars are provided.

1. Introduction

An era of deep imaging surveys of large areas of the sky has started with projects such as the Sloan Digital Sky Survey (SDSS), Pan-STARRS (PS), the Dark Energy Survey (DES), Skymapper, the Asteroid Terrestrial-impact Last Alert System (ATLAS), the All-Sky Automated Survey for Supernovae (ASAS-SN), the Zwicky Transient Facility (ZTF). Missions such as the Vera Rubin Observatory (VRO) and the Nancy Grace Roman Space Telescope are only a few of years away. Other facilities such as Gaia, Kepler, and TESS report the photometry of millions of stars to very high internal accuracy. All these projects

have their own native photometric system, with some of them differing significantly. To make the astrophysical information across these missions and surveys commensurate with one another, they must be put on a common photometric system by relying on a set of calibration references.

Sub-percent global photometric standardization has been challenging in the past, but is now in high demand for several ongoing scientific studies. For instance, photometric calibration is the major source of uncertainty in the use of Type Ia supernovae as probes of the history of cosmic expansion to infer the properties of the dark energy (Betoule et al. 2014; Scolnic et al. 2015, 2019, 2022; Stubbs & Brown 2015; Brout et al. 2022). Experiments that require accurate and reliable photoredshift determination, such as weak lensing tomography and baryonic acoustic oscillation analysis with the VRO (Gorecki et al. 2014), are also limited by systematic uncertainties arising from their relative photometric calibration.

A few years ago we started a project, led by A. Saha, to create a network of all-sky spectrophotometric standard DA
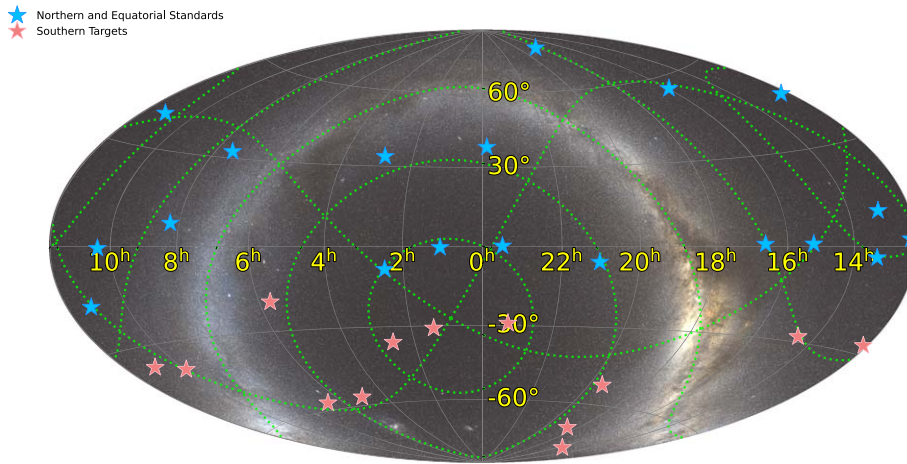
Figure 1. Hammer–Aitoff projection of our network of spectrophotometric standard DAWDs. This includes 19 DAWDs distributed in the Northern hemisphere and around the celestial equators (blue stars) and 13 in the Southern hemisphere (pink).

white dwarfs (DAWDs). The majority of these stars are fainter than $V \approx 18$ mag, i.e., bright enough to provide a good signal-to-noise ratio (S/N) while still avoiding saturation in existing and future deep surveys. We used Wide Field Camera 3 (WFC3) on the Hubble Space Telescope (HST) photometry collected in six filters from the near-ultra-violet (NUV) to the near-infrared (NIR) regime, ground-based spectroscopy, and hydrogen atmosphere white dwarf (WD) models to provide theoretical spectral energy distributions (SEDs) for all the DAWDs. 19 stars out of 23 candidates (blue stars in Figure 1), distributed around the celestial equators and in the Northern hemisphere, were established as standards in Calamida et al. (2019, hereafter CA19) and Narayan et al. (2019, hereafter NA19). Their SEDs agree with the multi-band HST photometry to better than 1% (see Figure 16 in NA19). These standards are tied to the HST photometric system, based on the spectro-photometry of the three CALSPEC primary DAWDs[16] (Bohlin 2014; Bohlin et al. 2020).

More recently, we collected ground-based spectroscopy, presented in the current paper, for candidate WDs in the Southern celestial hemisphere; on the basis of their spectra, 15 of them were selected to be subsequently observed with HST.[17] A companion paper describes how 13 of these DAWDs will be established as spectrophotometric standards (T. Axelrod et al. 2022, in preparation).

Our final goal is to provide an all-sky network of spectro-photometric standards so that at least two of these stars will be visible at any time from any observatory at an airmass of less than 2. The distribution of the established standards on the sky (19 in the Northern hemisphere and around the celestial equators, and 13 in the Southern hemisphere) is shown in the Hammer–Aitoff projection of Figure 1.

In addition to verifying the consistency of the spectroscopy and HST photometry with WD atmosphere models, we have monitored all the candidate spectrophotometric standard DAWDs for variability by collecting time-spaced data with the Las Cumbres Observatory (LCO) network of telescopes.[18] In CA19, we already showed how these data allowed us to identify two candidate standard DAWDs in the Northern

hemisphere, namely, SDSSJ203722.169-051302.964 and WD0554-165, as not stable. These were then excluded from our network of standards (CA19, NA19). This manuscript will illustrate the detailed analysis of the photometric monitoring data collected with LCO for all the candidate spectrophoto-metric standard DAWDs.

The structure of the paper is as follows. In Section 2, we present our sample of spectrophotometric standard DAWDs and in Section 3 we illustrate the time-monitoring observations and the photometric reduction procedures. In Section 4, we describe the variability analysis and Section 5 lists the details for each of the DAWDs. We summarize the results in Section 6. The appendices show the light curves for all the DAWDs observed with LCO and finding charts based on HST NIR images.

2. Candidate Spectrophotometric Standard Stars

DAWDs were selected from the SDSS (Adelman-McCarthy et al. 2008; Girven et al. 2012; Kleinman et al. 2013) and the Villanova catalog (McCook & Sion 1999) to uniformly cover the sky around the celestial equators and in the Northern hemisphere (Figure 1). For more details on the selection of these stars, we refer the reader to CA19. In the Southern hemisphere, there are relatively few faint WDs with prior spectroscopic identifications. Therefore, we relied on published lists of probable WDs based on color and proper motions selection such as those of Gentile-Fusillo et al. (2017) and Raddi et al. (2016, 2017), to establish candidate stars with suitable brightness and celestial placement. These works used photometry collected with the Very Large Telescope Survey Telescope ATLAS and VPHAS+ surveys and proper motions from the Absolute Proper motions Outside the Plane (APOP; Qi et al. 2015) catalog to identify WD candidates. For more details on the selection process please see the aforementioned manuscripts.

The original sample for the Northern hemisphere consisted of 23 DAWDs for which we presented the analysis of the HST photometry and ground-based spectroscopy in CA19. Of these, 19 DAWDs were established as standards in NA19. For the Southern hemisphere, we collected spectroscopy for a sample of 48 candidate DAWDs and selected 15 of them to be observed with HST and LCO. 13 of these will be established as standards in T. Axelrod et al. 2022, in preparation.

Table 1
Gaia DR3 Astrometry and Photometry for the Candidate Spectrophotometric Standard DAWDs

Star	Name	Alternative Name	Gaia DR3 ID	R.A.[a] (hh:mm:ss.s)	Decl.[a] (dd:mm:ss.s)	PM$_{R.A.}$ (mas yr^{-1})	PM$_{Decl.}$ (mas yr^{-1})	G (mag)	G_{RP} (mag)	G_{BP} (mag)
				Northern and equatorial DAWDs						
J0103-0020	WDFS0103-00	SDSSJ010322.19-002047.7	2536159496590552704	01:03:22.201	−00:20:47.800	6.196 ± 0.382	−6.550 ± 0.355	19.30	19.67	19.16
J0228-0827	WDFS0228-08	SDSSJ022817.16-082716.4	5176546064064586624	02:28:17.183	−08:27:16.301	10.916 ± 0.783	3.151 ± 0.539	19.97	20.07	19.82
J0248+3345	WDFS0248+33	SDSSJ024854.96+334548.3	139724391470489472	02:48:54.965	33:45:48.244	4.093 ± 0.253	−4.759 ± 0.205	18.52	18.74	18.42
J0410-0630[b]	...	SDSSJ041053.632-063027.580	3196384966004896640	04:10:53.641	−06:30:27.677	8.577 ± 0.279	9.719 ± 0.185	18.99	19.22	19.02
J0557-1635[b]	...	WD0554-165	2991789869534666240	05:57:01.292	−16:35:12.159	−6.747 ± 0.099	4.272 ± 0.101	17.94	18.40	17.83
J0727+3214	WDFS0727+32	SDSSJ072752.76+321416.1	892231562565363072	07:27:52.752	32:14:16.046	−13.151 ± 0.168	−6.923 ± 0.128	18.19	18.45	18.04
J0815+0731	WDFS0815+07	SDSSJ081508.78+073145.7	3097940536010212736	08:15:08.782	07:31:45.775	5.519 ± 0.811	−0.190 ± 0.733	19.93	20.25	19.79
J1024-0032	WDFS1024-00	SDSSJ102430.93-003207.0	3830980604624181376	10:24:30.912	−00:32:07.160	−21.301 ± 0.388	−5.670 ± 0.590	19.08	19.23	19.00
J1110-1709	WDFS1110-17	SDSSJ111059.42-170954.2	3559181712491390208	11:10:59.436	−17:09:54.308	5.454 ± 0.162	−8.015 ± 0.136	18.05	18.37	17.91
J1111+3956	WDFS1111+39	SDSSJ111127.30+395628.0	765355922242992000	11:11:27.313	39:56:28.105	2.734 ± 0.231	2.933 ± 0.255	18.64	19.07	18.48
J1206+0201	WDFS1206+02	SDSSJ120650.504+020143.810	3891742709551744640	12:06:50.410	02:01:42.138	−5.061 ± 0.300	−23.367 ± 0.149	18.85	19.07	18.75
J1214+4538	WDFS1214+45	SDSSJ121405.11+453818.5	1539041748873288704	12:14:05.111	45:38:18.626	0.278 ± 0.088	13.925 ± 0.104	17.98	18.23	17.84
J1302+1012	WDFS1302+10	SDSSJ130234.43+101238.9	3734528631432609920	13:02:34.422	10:12:38.717	−12.856 ± 0.132	−16.837 ± 0.122	17.24	17.54	17.10
J1314-0314	WDFS1314-03	SDSSJ131445.050-031415.588	3684543213630134784	13:14:45.046	−03:14:15.685	−3.930 ± 0.404	−5.659 ± 0.265	19.31	19.74	19.25
J1514+0047	WDFS1514+00	SDSSJ151421.27+004752.8	4419865155422033280	15:14:21.277	00:47:52.380	4.350 ± 0.059	−26.855 ± 0.053	15.88	16.11	15.77
J1557+5546	WDFS1557+55	SDSSJ155745.40+554609.7	1621657158502507520	15:57:45.380	55:46:09.361	−11.677 ± 0.112	−21.478 ± 0.126	17.69	18.04	17.53
J1638+0047	WDFS1638+00	SDSSJ163800.360+004717.822	4383979187540364288	16:38:00.352	00:47:17.739	−9.171 ± 0.320	−2.737 ± 0.239	19.02	19.36	18.91
J1721+2940[b]	...	SDSSJ172135.97+294016.0	4599419007715436928	17:21:35.951	29:40:16.178	−20.919 ± 0.230	10.536 ± 0.26	19.60	19.50	19.69
J1814+7854	WDFS1814+78	SDSSJ181424.075+785403.048	2293913930823813888	18:14:24.078	78:54:03.084	−10.738 ± 0.060	11.535 ± 0.057	16.74	17.03	16.61
J2037-0513[b]	...	SDSSJ203722.169-051302.964	6908492038494775680	20:37:22.173	−05:13:03.023	3.118 ± 0.267	−2.000 ± 0.206	19.11	19.40	19.04
J2101-0545	WDFS2101-05	SDSSJ210150.65-054550.9	6910475935427725824	21:01:50.667	−05:45:51.159	9.984 ± 0.218	−11.694 ± 0.210	18.83	19.10	18.74
J2329+0011	WDFS2329+00	SDSSJ232941.330+001107.755	2644572064644349952	23:29:41.321	00:11:07.565	−7.982 ± 0.189	−14.919 ± 0.162	18.29	18.42	18.24
J2351+3755	WDFS2351+37	SDSSJ235144.29+375542.6	2881271732415859072	23:51:44.274	37:55:42.569	−16.412 ± 0.145	−9.941 ± 0.107	18.23	18.50	18.12
				Southern DAWDs						
J0122-3052	WDFS0122-30	ATLAS020.503022	5028544686500198144	01:22:00.725	−30:52:03.950	20.621 ± 0.14	−12.303 ± 0.135	18.66	19.01	18.53
J0238-3602	WDFS0238-36	SSSJ023824	4953936951336477440	02:38:24.969	−36:02:23.222	57.993 ± 0.078	13.747 ± 0.119	18.24	18.39	18.19
J0419-5319[b]	...	WD0418-534	4779427928974390272	04:19:24.608	−53:19:16.659	−17.587 ± 0.048	27.166 ± 0.063	16.42	16.69	16.30
J0458-5637	WDFS0458-56	SSSJ045822	4764189621230467584	04:58:23.133	−56:37:33.434	143.596 ± 0.118	66.486 ± 0.13	17.96	18.25	17.85
J0541-1930	WDFS0541-19	SSSJ054114	2967083052984612736	05:41:14.759	−19:30:38.896	19.248 ± 0.126	−26.954 ± 0.142	18.43	18.61	18.35
J0639-5712	WDFS0639-57	SSSJ063941	3486471764460448512	06:39:41.468	−57:12:31.164	17.513 ± 0.126	43.576 ± 0.151	18.37	18.70	18.27
J0757-6049[b]	...	WD0757-606	5484605140287436416	07:57:50.637	−60:49:54.634	−4.590 ± 0.287	11.067 ± 0.223	18.95	19.15	18.89
J0956-3841	WDFS0956-38	SSSJ095657	5290720695823013376	09:56:57.009	−38:41:30.269	−8.269 ± 0.084	−46.075 ± 0.092	18.00	18.16	17.94
J1055-3612	WDFS1055-36	SSSJ105525	5421579652019276160	10:55:25.356	−36:12:14.731	−21.353 ± 0.124	46.134 ± 0.119	18.20	18.45	18.12
J1206-2729	WDFS1206-27	WD1203-272	5401230062610609920	12:06:20.354	−27:29:40.639	3.019 ± 0.074	2.796 ± 0.081	16.67	16.93	16.54
J1434-2819	WDFS1434-28	SSSJ143459	6222123588482712832	14:34:59.528	−28:19:03.295	−48.559 ± 0.206	18.600 ± 0.195	18.10	18.35	18.07
J1535-7724	WDFS1535-77	WD1529-772	5779908502946006784	15:35:45.179	−77:24:44.832	−26.881 ± 0.055	−43.749 ± 0.058	16.76	17.09	16.60
J1837-7002	WDFS1837-70	SSSJ183717	6431766714636858240	18:37:17.906	−70:02:52.513	10.378 ± 0.072	−75.989 ± 0.106	17.91	18.08	17.85
J1930-5203	WDFS1930-52	SSSJ193018	6646236009641999488	19:30:18.995	−52:03:46.550	21.546 ± 0.123	−33.286 ± 0.102	17.67	17.94	17.55
J2317-2903	WDFS2317-29	WD2314-293	2378059688840742912	23:17:20.294	−29:03:21.647	3.991 ± 0.146	25.051 ± 0.196	18.53	18.81	18.44

Notes. Stars are divided into the Northern and Equatorial and Southern samples and listed in order of increasing R.A.
[a] Coordinates are from Gaia DR3 at epoch 2016.0 precessed to J2000.0, no proper motion applied. To get current coordinates apply the proper motions from 2016 and precess.
[b] This star was excluded from the final network of spectrophotometric standard DAWDs. See text for more details.

(This table is available in machine-readable form.)

Table 1 lists the 38 (23 + 15) DAWDs of the original sample, with HST, ground-based spectra, and LCO observations, and provides their name (with the *J* designation plus the 4 digits of Gaia Data Release 3 (DR3, Gaia Collaboration et al. 2022) R.A. and decl. coordinates at epoch 2016.0 precessed to J2000.0), a new name for the 32 (19 + 13) stars established as spectrophotometric standards, the alternative name, and the IDs, coordinates, proper motions, and photometry from Gaia DR3. Gaia magnitudes are provided to illustrate the brightness range of our candidate spectrophotometric standards. A discussion on the comparison between Gaia DR3 magnitudes and synthetic Gaia magnitudes derived for our entire sample of DAWDs is deferred to T. Axelrod et al. 2022, in preparation.

We assigned new names to the 32 established spectrophotometric standard DAWDs: these are composed of the *White Dwarf Flux Standard* (WDFS) designation and 4 digits of the R.A. and 2 of the decl. coordinates from Gaia DR3 as their ID number. The new names are listed in the third column of Table 1.

In Appendix C, we provide finding charts for all 38 DAWDs. These are based on HST images collected in the F160W filter during our observing programs. We selected this filter since some possibly contaminant faint red sources become visible in the infrared regime.

2.1. Spectroscopy of the Candidate Spectrophotometric DAWDs

Spectra of the Northern sample of DAWDs were collected with the Gemini Multi-Object Spectrograph (GMOS; Hook et al. 2004) mounted on the Gemini North and South telescopes. However, due to issues with the quality of the GMOS spectra, further observations were collected with the Blue Channel spectrograph at the MMT Observatory. Details on these data and their reduction and analysis were presented in CA19.

Spectra of 48 Southern candidate WDs were obtained with the Goodman spectrograph (Clemens et al. 2004) on the 4 m SOAR telescope (NOIRLab). Exposures were collected for each star and some were observed multiple times between 2016 February and 2017 February. The log of the observations is provided in Table 2 and includes the star name (with the *J* designation plus the 4 digits of Gaia DR3 R.A. and decl.), the alternative name, Gaia DR3 IDs, and coordinates.

All the spectra were visually inspected and non-DAWD stars and stars with obvious spectroscopic peculiarities or magnetic activity were rejected. We ended up with 15 candidate spectrophotometric standard DAWDs that we observed with WFC3/HST and monitored for stability with LCO.

For the SOAR spectroscopic observations, we used the 1″07 slit, oriented at the parallactic angle, where possible. Spectra were reduced and processed by following the same technique used for the Northern DAWD sample as described in CA19. The final spectra have a typical range of 3850–7100 Å with an intrinsic dispersion of 1.99 Å per pixel, re-binned to 2 Å per pixel for the final spectra. Figures 2–5 show the spectra of all the candidate WDs that were observed in the Southern hemisphere. The first figure shows the 13 DAWDs with HST and LCO observations that were established as spectrophotometric standards, while the other three figures show objects that were discarded for various reasons. In particular, Figure 5 displays six objects with unusual spectra: the top plot shows a strong blue featureless spectrum, possibly a hot DC WD, while the second and third ones are blue He-rich spectra, possibly DB degenerates. The remaining spectra in the figure show Zeeman splitting of the Balmer lines indicating magnetic degenerates.

2.2. Stability of the Spectrophotometric Standard DAWDs

In order to assess the DAWDs as stable standards we monitored them by collecting time-spaced data with the LCO network of telescopes. WDs can vary due to several reasons, depending on their effective temperature, atmosphere abundance, and presence of magnetic activity or of an unseen faint companion star.

Hydrogen-rich atmosphere WDs might present gravity-mode pulsations around $T_{\rm eff} \sim 12{,}000$ K (Fontaine & Brassard 2008, ZZ Ceti pulsators). Our DAWDs were selected to have temperatures ($T_{\rm eff} \gtrsim 20{,}000$ K) outside the ZZ Ceti instability strip, so we do not expect them to be pulsators (note that SDSSJ172135.97+294016.0 was removed from the network of standards as its temperature is $T_{\rm eff} = 9261$ K, see CA19, NA19). Strong magnetic fields can also cause flux variations in WDs with a timescale from hours to days. These variations can be due to magnetically confined "spots" of higher opacity modulating the stellar flux via stellar rotation (Dupuis et al. 2000; Holberg & Howell 2011). Alternately, magnetic variations can be due to spots in the convective atmosphere (Brinkworth et al. 2004, 2013). However, our candidate standard DAWDs have effective temperatures above $\sim 20{,}000$ K, and their atmosphere is fully radiative, so they should not vary due to the presence of spots. Furthermore, we excluded candidates with spectra showing Zeeman splitting of the Balmer lines indicative of the presence of a strong magnetic field (see Figure 5).

On the other hand, the selected DAWDs could still vary due to the presence of an unseen faint companion star, for example, and we need to characterize the amount of flux variation, if present, before setting these stars as spectrophotometric standards.

A study by Hermes et al. (2017), based on precise Kepler time-series photometry, showed that $\sim 97\%$ of apparently isolated WDs are stable, or show less than 1% flux variations, and they can be used as spectrophotometric standards. Hermes et al. sample included mostly DAWDs but also several helium- or carbon-dominated atmosphere WDs, with temperatures hotter than ~ 8000 K.

By comparing observations and binary population synthesis models, Toonen et al. (2017) studied the binarity of the almost complete local WD sample ($d \lesssim 20$ pc). Assuming an initial binary fraction of 50%, these models show that most systems undergo a common envelope phase and subsequent merger with the final outcome of $\sim 70\%$–80% of WDs being isolated. The remaining fraction of systems are probably on a wide orbit, as these binaries can more easily avoid the common envelope-merger phase, and can be observed as resolved binaries. These systems are usually separated by a few arcseconds. Our DAWDs are more distant than the local sample, $100 \lesssim d \lesssim 1000$ pc, but WFC3 detectors' spatial resolution would easily allow us to resolve the companions (pixel scales of $\sim 0{.}^{\prime\prime}04$ and $0{.}^{\prime\prime}13$ for the UVIS and the IR camera, respectively, resulting in separations of more than a dozen pixels in both cases). The same models from Toonen et al. (2017) predict a fraction of $\sim 0.5\%$–1% of unresolved binaries. For most of these, the companion would be

Table 2
Log of the Observations Collected with the Goodman Spectrograph on the 4 m SOAR Telescope NOAO Programs 2017A-0052 (PI: Olszewski)

Star	Alternative Name	Gaia DR3 ID	R.A.[a] (hh:mm:ss.s)	Decl.[a] (dd:mm:ss.s)	UT Date	Range (Å)	P.A. (°)	Air.	Flux Std.	Exp. (s)
J0122-3052	ATLAS020.503022	5028544686500198144	01:22:00.725	−30:52:03.950	2016-10-7	3870–7100	263.0	1.1	Feige110	4 × 900
J2140-3231	ATLAS325.224509-32.5	6592388973858801920	21:40:53.887	−32:31:17.381	2016-10-5	3870–7100	90.0	1.1	Feige110	3 × 900
J2214-2954	ATLAS333.686598	6614900207422023168	22:14:44.788	−29:54:37.641	2016-10-6	3870–7100	261.0	1.1	Feige110	900
J2242-2913	ATLAS340.6628	6608532725132112768	22:42:39.087	−29:13:16.348	2016-10-7	3870–7100	260.0	1.1	Feige110	4 × 900
J2343-3732	ATLAS355.86084	6538080044408150784	23:43:26.600	−37:32:36.724	2016-10-6	3870–7100	60.0	1.0	Feige110	4 × 900
J0025-2840	ATLAS6.345142	2321781186172842624	00:25:22.838	−28:40:33.944	2016-10-6	3870–7100	100.0	1.1	Feige110	3 × 900
J1800-2332	RU139-WD	4069124858877707776	18:00:42.030	−23:32:38.652	2016-10-5	3870–7100	112.0	1.3	Feige110	4 × 900
J0141-6140	SSSJ014151	4712803636068739456	01:41:51.827	−61:40:48.350	2016-10-7	3870–7100	298.0	1.3	Feige110	900
J0215-6127	SSSJ021508	4713619542415902336	02:15:08.335	−61:27:30.571	2016-10-5	3870–7100	321.0	1.2	Feige110	4 × 900
J0226-2214	SSSJ022634	5120586282330070784	02:26:34.644	−22:14:22.824	2016-10-6	3870–7100	130.0	1.0	Feige110	3 × 900
J0238-3602	SSSJ023824	4953936951336477440	02:38:24.969	−36:02:23.222	2016-10-7	3870–7100	273.0	1.1	Feige110	4 × 900
J0301-2450	SSSJ030158	5074738090560529792	03:01:58.400	−24:50:44.068	2016-10-7	3870–7100	243.0	1.0	Feige110	3 × 900
J0328-2839	SSSJ032813	5056979122346336384	03:28:13.113	−28:39:25.621	2017-02-22	3850–7100	102.0	1.3	Feige67	1000
J0358-7559	SSSJ035817	4628635093249821952	03:58:17.886	−75:59:29.089	2016-10-7	3870–7100	243.0	1.0	Feige110	3 × 900
J0343-2556	SSSJ034259	5082086886979911424	03:43:04.171	−25:56:55.110	2016-02-12	3850–7150	60.0	1.1	Feige67	2 × 900
J0343-2556	SSSJ034259	5082086886979911424	03:43:04.171	−25:56:55.110	2016-02-12	3850–7150	60.0	1.2	Feige67	3 × 1200
J0358-7559	SSSJ035817	4628635093249821952	03:58:17.886	−75:59:29.089	2016-02-11	3850–7150	58.0	1.5	Feige67	2 × 1200
J0450-2846	SSSJ045030	4879984623886489600	04:50:30.966	−28:46:02.222	2017-02-23	3850–7100	100.0	1.1	GD71	2 × 1200
J0458-5637	SSSJ045822	4764189621230467584	04:58:23.133	−56:37:33.434	2016-10-6	3870–7100	339.0	1.1	Feige110	3 × 900
J0458-5637	SSSJ045822	4764189621230467584	04:58:23.133	−56:37:33.434	2017-02-22	3850–7100	58.0	1.2	Feige67	3 × 1000
J0512-3112	SSSJ051210	4827685043344935168	05:12:10.898	−31:12:59.861	2016-10-5	3870–7100	265.0	1.1	Feige110	5 × 900
J0541-1930	SSSJ054114	2967083052984612736	05:41:14.759	−19:30:38.896	2016-10-7	3870–7100	244.0	1.2	Feige110	3 × 900
J0633-7858	SSSJ063322	5211173052478517120	06:33:22.458	−78:58:19.125	2017-02-22	3850–7100	31.0	1.6	Feige67	3 × 1200
J0639-5712	SSSJ063941	5484605140287436416	06:39:41.468	−57:12:31.164	2016-10-7	3870–7100	303.0	1.2	Feige110	3 × 900
J0639-5712	SSSJ063941	5484605140287436416	06:39:41.468	−57:12:31.164	2017-02-23	3850–7100	24.0	1.2	GD71	3 × 1200
J0947-8458	SSSJ094704	5191604494282635136	09:47:02.983	−84:58:39.558	2016-02-10	3850–7150	5.0	1.7	Feige67	4 × 1200
J0956-3841	SSSJ095657	5421579652019276160	09:56:57.009	−38:41:30.269	2017-02-22	3850–7100	334.0	1.0	Feige67	3 × 1200
J0957-0019	SSSJ095749	3833430797566676352	09:57:49.372	−00:19:49.381	2017-02-23	3850–7100	136.0	1.5	GD71	3 × 1200
J1002-8031	SSSJ100248	5201701240840634624	10:02:49.314	−80:31:10.614	2016-02-12	3850–7150	348.0	1.6	Feige67	2 × 1200
J1002-8031	SSSJ100248	5201701240840634624	10:02:49.314	−80:31:10.614	2016-02-12	3850–7150	30.0	1.6	Feige67	2 × 900
J1055-3612	SSSJ105525	5401230062610609920	10:55:25.356	−36:12:14.731	2017-02-23	3850–7100	11.0	1.0	GD71	3 × 1200
J1101-3621	SSSJ110129	5400333861851343616	11:01:29.850	−36:21:04.362	2017-03-18	3850–7150	75.0	1.1	…	2 × 1200
J1159-5008	SSSJ115943	5370694601787409152	11:59:43.451	−50:08:18.370	2017-03-18	3850–7150	334.0	1.1	…	2 × 1200
J1212-4029	SSSJ121247	6149314478246925056	12:12:47.130	−40:29:46.827	2017-02-22	3850–7100	295.0	1.1	Feige67	3 × 1200
J1434-2819	SSSJ143459	6222123588482712832	14:34:59.528	−28:19:03.295	2017-02-22	3850–7100	257.0	1.1	Feige67	3 × 1200
J1837-7002	SSSJ183517	6431766714636858240	18:37:17.906	−70:02:52.513	2016-10-6	3870–7100	44.0	1.4	Feige110	3 × 900
J1930-5203	SSSJ193018	6646236009641999488	19:30:18.995	−52:03:46.550	2016-10-6	3870–7100	64.0	1.2	Feige110	3 × 900
J1947-3100	SSSJ194736	6751474223204472576	19:47:36.361	−31:00:39.385	2016-10-4	3870–7100	95.0	1.1	Feige110	3 × 900
J2023-4015	SSSJ202344	6680866227868812288	20:23:44.526	−40:15:21.092	2016-10-6	3870–7100	84.0	1.2	Feige110	3 × 900
J2220-4645	SSSJ222035	6518394383932274432	22:20:36.053	−46:45:52.384	2016-10-6	3870–7100	60.0	1.1	Feige110	900
J0054-2650	WD0052-271	2344195005582967040	00:54:57.994	−26:50:23.221	2016-10-5	3870–7100	106.0	1.0	Feige110	3 × 900
J0259-2805	WD0257-282	5071554695160551040	02:59:23.254	−28:05:33.327	2016-02-11	3850–7150	105.0	1.2	Feige67	3 × 1200
J0419-5319	WD0418-534	4779427928974390272	04:19:24.680	−53:19:16.659	2017-02-22	3850–7100	62.0	1.2	Feige67	3 × 600
J0512-4145	WD0510-418	4812859061053900928	05:12:23.053	−41:45:26.057	2016-02-10	3850–7150	40.0	1.0	Feige67	4 × 600
J0757-6054	WD0756-607	5290719287073728128	07:57:03.112	−60:54:52.622	2016-02-11	3850–7150	27.0	1.2	Feige67	3 × 1200
J0757-6049	WD0757-606.2	5290720695823013376	07:57:50.637	−60:49:54.634	2016-02-10	3850–7150	338.0	1.2	Feige67	4 × 1200
J1105-5852	WD1103-586.1	5338652084186678400	11:05:35.811	−58:52:26.385	2016-02-11	3850–7150	345.0	1.2	Feige67	3 × 1200

Table 2
(Continued)

Star	Alternative Name	Gaia DR3 ID	R.A.[a] (hh:mm:ss.s)	Decl.[a] (dd:mm:ss.s)	UT Date	Range (Å)	P.A. (°)	Air.	Flux Std.	Exp. (s)
J1105-5829	WD1103-582	5340167657872411520	11:05:53.071	−58:29:31.090	2016-02-10	3850–7150	8.0	1.2	Feige67	4 × 1200
J1146-3141	WD1143-314	3479327447141240320	11:46:18.107	−31:41:01.612	2016-02-11	3850–7150	85.0	1.0	Feige67	3 × 600
J1146-3141	WD1143-314	3479327447141240320	11:46:18.107	−31:41:01.612	2017-02-23	3850–7100	96.0	1.2	GD71	2 × 420
J1206-2729	WD1203-272	3486471764460448512	12:06:20.354	−27:29:40.639	2016-02-11	3850–7150	105.0	1.0	Feige67	3 × 600
J1206-2729	WD1203-272	3486471764460448512	12:06:20.354	−27:29:40.639	2017-02-22	3850–7100	103.0	1.1	Feige67	2 × 300
J1535-7724	WD1529-772	5779908502946006784	15:35:45.179	−77:24:44.832	2016-02-12	3850–7150	320.0	1.6	Feige67	2 × 900
J2317-2903	WD2314-293	2378059688840742912	23:17:20.294	−29:03:21.647	2016-10-5	3870–7100	81.0	1.0	Feige110	3 × 900
J2317-2918	WD2315-295	2330002990527676800	23:17:58.479	−29:18:19.535	2016-10-7	3870–7100	261.0	1.1	Feige110	3 × 900

Notes. Every row corresponds to a different visit. Observations are sorted by survey and by increasing R.A. values.

[a] Coordinates are from Gaia DR3 at epoch 2016.0 precessed to J2000.0, no proper motion applied. To get current coordinates apply the proper motions from 2016 and precess.

(This table is available in machine-readable form.)
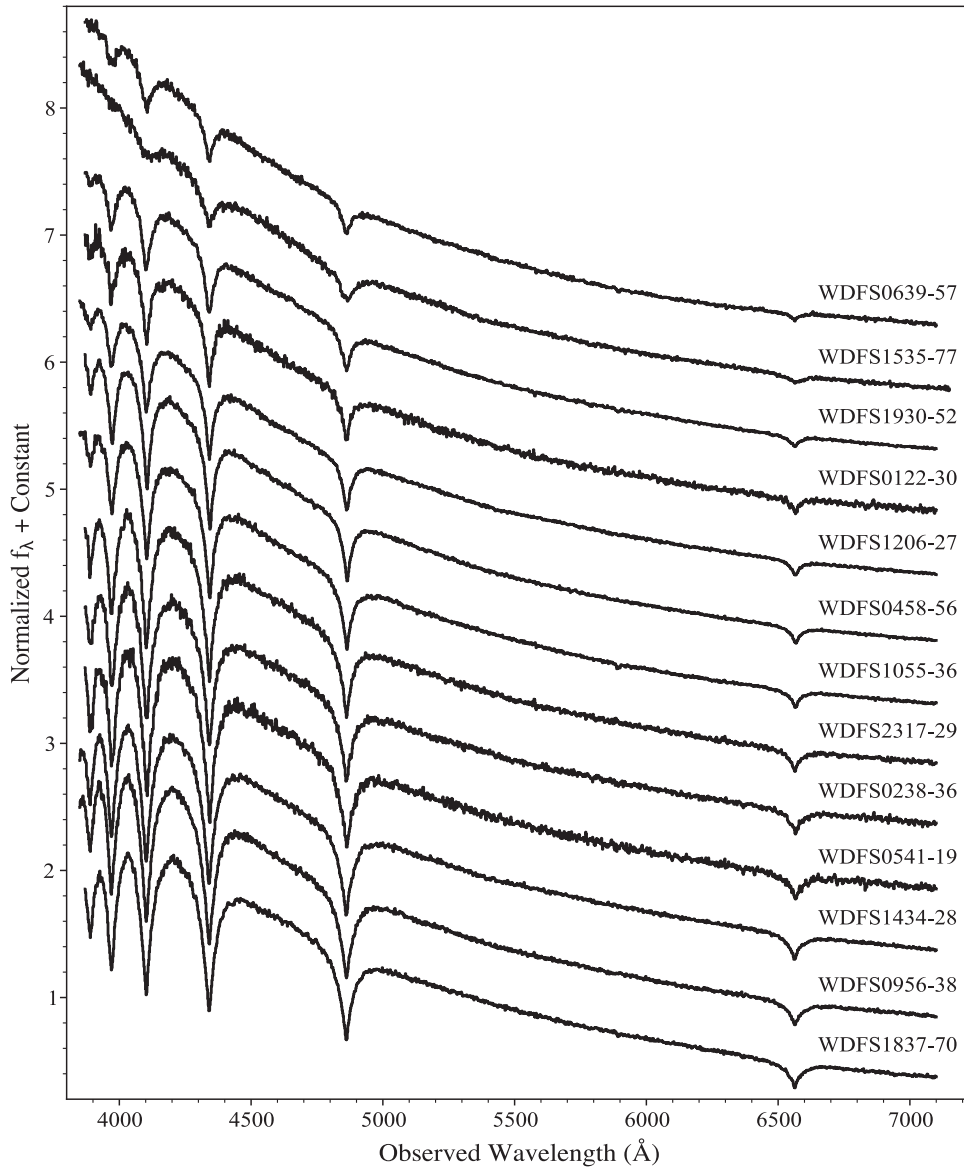
Figure 2. Spectra collected with the Goodman spectrograph on the 4 m SOAR telescope (NOIRLab) for the 13 confirmed spectrophotometric standard DAWDs with HST and LCO follow-up observations.

identified through spectroscopy, such as for SDSSJ203722.169-051302.964, where spectra showed an emission feature in the cores of the Balmer absorption lines, probably the result of a low-luminosity companion or some other activity associated with the DAWD. The variability of this star was also confirmed by the analysis of the LCO time-spaced observations (see discussion in Section 4). However, if the companion to the DAWD is a faint red dwarf, then current spectroscopy is not able to detect it, and not even imaging at the spatial resolution of HST. That is why we started a photometric monitoring campaign.

On the basis of the criteria used to select our set of DAWDs and the evidence from the WFC3 and spectroscopic data, we do not expect a large fraction of our candidate spectrophotometric standards to vary. However, these DAWDs have not yet been subject to a consistent and well-defined observational campaign to demonstrate a lack of variability at a wide range of timescales. WFC3 observations are obtained within a short time frame for each target, so they are unsuitable as tests of variation. Ground-based surveys (SDSS, PS, ATLAS) and space facilities (Kepler, TESS)

also do not have the necessary temporal coverage or spatial resolution, and Gaia does not provide variability constraints on these stars yet.

3. Time-spaced Observations

Time-spaced data for 23 candidate spectrophotometric standard DAWDs in the Northern hemisphere and around the celestial equators were collected with LCO starting in the fall of 2016 until the summer of 2017, for a total of ∼1 yr of observations.[19] A few exposures were also collected in the first semester of 2018,[20] to add more epochs to some targets. Observations for the 15 candidates in the Southern hemisphere were collected in a semester in 2018 and one in 2019.[21]

Data consist of a sequence of exposures in the Sloan g filter, separated by minutes up to a month in time. A minimum of 20

---

[19] LCO2016B-007 and LCO2017AB-002 (PI: Matheson).
[20] LCO2018A-002 (PI: Matheson).
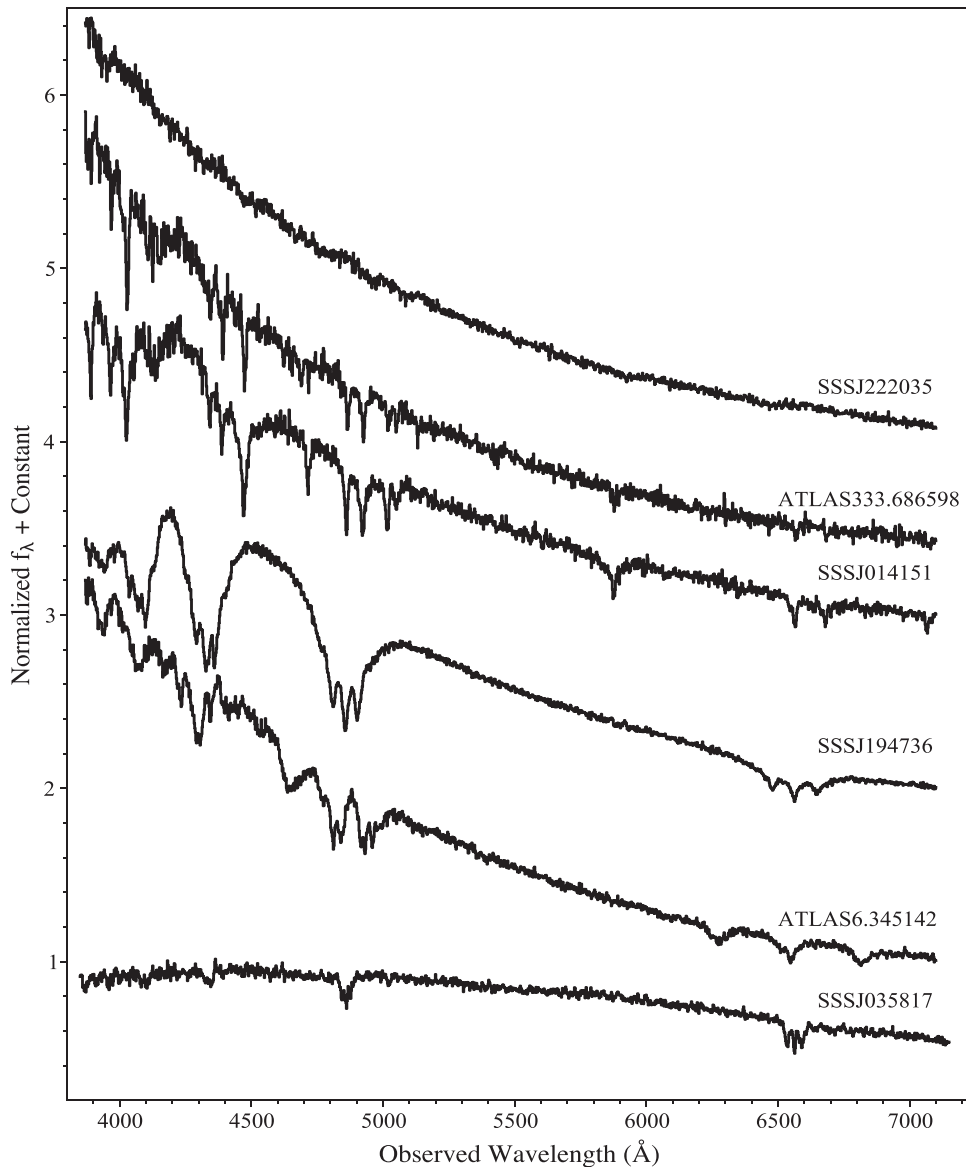[21] LCO2018B-001 and LCO2019-B004 (PI: Matheson).
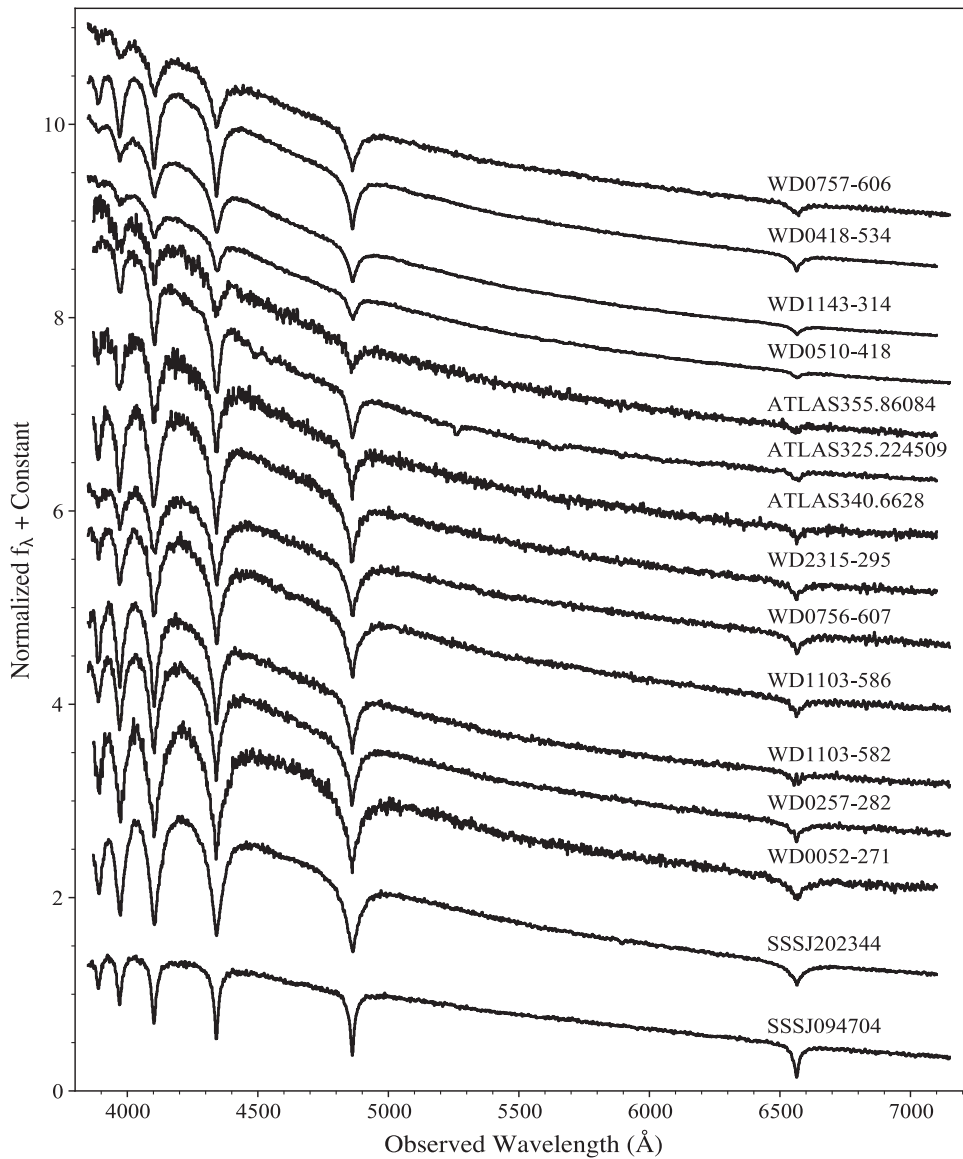
Figure 3. Spectra collected with the Goodman spectrograph on the 4 m SOAR telescope (NOIRLab) for candidate DAWDs that were discarded from the Southern hemisphere sample (continues in Figure 4). The first and second star, WD0756-607 and WD0418-534, were excluded from our network of standards due to their variability and other reasons. See text for more details.

exposures for each target were collected, spread over 2–3 months at different time intervals, for a total of ≈1400 images. The log of the observations is shown in Table 3.

In order to schedule our observations at the LCO observatory, we developed a `python` routine that calculates the observing window for each star on the different network telescopes during a selected semester and the optimal exposure time to reach an $S/N \approx \times 100$. This code is available on GitHub at the following URL.[22]

3.1. Data Processing and Reduction

We downloaded all images collected for our programs from the LCO archive. These are processed by the BANZAI pre-reduction pipeline.[23] The pipeline performs a bad-pixel masking, bias and dark subtraction, and a flat-field correction.

It also provides an astrometric solution for the images and extracts aperture photometry for the sources by using Source Extractor (Bertin & Arnouts 1996). For more details please refer to the LCO BANZAI pipeline web page.[24]

Images were collected under different conditions, effectively being spread over different nights and months and utilizing different telescopes and observatories. All data were collected with the Sinistro 4K × 4K cameras mounted on the 1 m class network of telescopes. This includes Siding Spring (observatory code, COJ), Sutherland (CPT), Cerro Tololo Cerro Tololo Inter-American Observatory (LSC), and McDonald (ELP). The Sinistro cameras provide a total field of view (FoV) of ~26′ × 26′ with a pixel scale of 0″389. Seeing for the different observations for all DAWDs ranged between 1″7 and 2″5 on the images, with an average seeing ≈2″.

As a first step, the average FWHM for each frame was derived from the available Source Extractor photometry. To
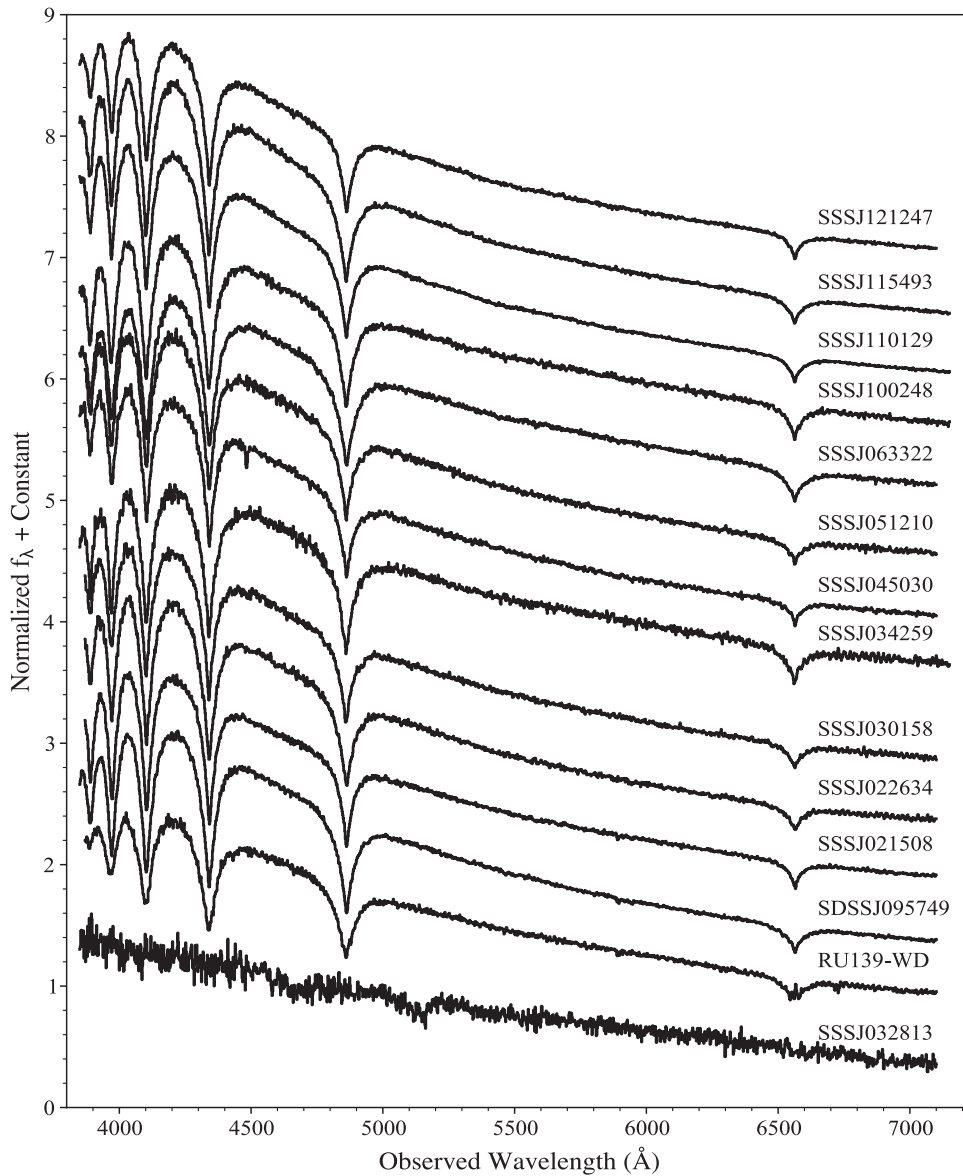
Figure 4. Same as Figure 3 but for different candidate DAWDs discarded from our Southern hemisphere sample. The last star could be a DQWD, showing the $C2$ Swan band at $\lambda \approx 5150$ Å.

exclude observations affected by poor observing conditions or bad focus, all the images with FWHM $\geqslant 7.5$ pixels (2″9) were discarded.

We then performed aperture photometry with DAOPHOTIV (Stetson 1987), using an aperture radius of 5 pixels, and the sky background was calculated in an annulus with radii of 7 and 20 pixels. Starting from the aperture photometry, we performed point-spread function (PSF) photometry with DAOPHOTIV/ ALLSTAR. An automatic pipeline was developed in python to run the different routines of DAOPHOT and derive a PSF for each image. The result is a sample of moderately bright, isolated, and well-measured PSF stars per image. The pipeline also runs ALLSTAR, i.e., the PSF-fitting routine, on all the images and produces a catalog with identified sources, coordinates, and magnitudes for every single image. Images that failed the automatic procedure were individually visually inspected and checked for problems. Most frequently they were out of focus or affected by clouds.

As a second step, we identified the best image (smallest average FWHM) for a set of exposures for each target and established it as a reference frame. This process is needed to flux scale all the photometric catalogs and to register all the exposures to the same coordinate system. In order to derive transformations between the images we used DAOMATCH/ DAOMASTER (Stetson 1994) and created a master catalog for each FoV. We then used the code ALLFRAME (Stetson 1994) to perform simultaneous PSF-fitting photometry on all images available for a target. ALLFRAME output catalogs were matched to derive light curves for all the stars in the observed FoV, including the DAWDs. Note that exposures for each target were flux scaled to the reference images to take into account effects due to the differences in the PSF, observing conditions, and exposure times. It is important to note that we are interested in relative and not absolute photometry, and the derived light curves for our DAWDs and all stars in the same FoV are not calibrated.

Figure 5. Spectra collected with the Goodman spectrograph on the 4 m SOAR telescope (NOIRLab) for candidate DAWDs that were discarded from our Southern hemisphere sample. The first star is featureless and could be a DC WD, the second and third could be DB degenerates. The last three are magnetic WDs.

We ended up with 38 final photometric catalogs, one for each DAWD star. On average, catalogs include ≈300–1000 stars distributed over the FoV. The DAWDs were identified in the final photometric catalogs by searching around their position (R.A., decl.) within a radius of 0°.001.

The data were also independently measured with the DoPHOT program (Schechter et al. 1993), using a process described in Saha et al. (2019). This produces a list of aperture-corrected instrumental magnitudes for each image. The lists for all images in the g band centered on any given target DAWD star were then matched by position (R.A., decl.). A single zero-point adjustment in instrumental magnitudes was applied to each list, so that the error-weighted ensemble average instrumental magnitudes of all matched objects were made the same across all images/epochs centered on the DAWD star. This assumes that the majority of stars on the frame are non-variable, thus putting all instrumental magnitudes for any given DAWD star field on the same footing. The results were written into an SQL database. Then, for any star in the field, the variability can be tested by extracting its measurements at all epochs, as described in the following section.

4. Variability Analysis

Measurements obtained with DoPHOT were used to calculate a reduced χ^2 for each star in a given FoV as

$$\chi^2 = \frac{\sum_{i=1}^{n} \frac{(m_i - \bar{m})^2}{\text{err}_i^2}}{n - 1}, \tag{1}$$

where m_i are the individual measurements, $\bar{m}$ is the mean weighted magnitude of each identified object, and err_i is the error on the individual measurements. The error estimates were those furnished by DoPHOT and propagated through the ensuing process. For robustness, for each star, multiple values of χ^2s were calculated using a bootstrap process. If, for

Table 3
Log of the Observations Collected with LCO during Programs LCO2016B-007, LCO2017AB-002, LCO2018A-002, LCO2018B-001, and LCO2019-B004
(PI: T. Matheson)

Star	Code[a]	R.A.[b] (hh:mm:ss.s)	Decl.[b] (dd:mm:ss.s)	MJD	Exposure Time (s)
WDFS1314-03	fl15	13:14:45.050	−03:14:15.64	57832.3508	304
WDFS1314-03	fl06	13:14:45.050	−03:14:15.64	57832.1	304
WDFS1314-03	fl06	13:14:45.047	−03:14:15.65	57960.7696	423
WDFS1314-03	fl04	13:14:45.050	−03:14:15.64	57832.2853	304
WDFS1314-03	fl04	13:14:45.050	−03:14:15.64	57832.2163	304
WDFS1314-03	fl14	13:14:45.050	−03:14:15.64	57842.9781	304
WDFS1314-03	fl03	13:14:45.047	−03:14:15.65	58143.3084	349
WDFS1314-03	fl03	13:14:45.047	−03:14:15.65	58160.2109	349
WDFS1314-03	fl15	13:14:45.050	−03:14:15.64	57832.3548	304
WDFS1314-03	fl15	13:14:45.050	−03:14:15.64	57832.2018	304
WDFS1314-03	fl04	13:14:45.050	−03:14:15.64	57832.2918	304
WDFS1314-03	fl06	13:14:45.050	−03:14:15.64	57832.096	304

Notes.
[a] Telescope code.
[b] Coordinates are at epoch J2000.

(This table is available in its entirety in machine-readable form.)

instance, there were n measurements available, we constructed a sample of n measurements by randomly picking from the available measurements with replacement, and take the average of all the ensuing χ^2 values. The resulting reduced χ^2s for each object in a given field were plotted against instrumental magnitude to visually de-trend the effects of miss-estimation of the errors and make variable objects stand out in this diagram.

Since the data were taken at various telescopes of the LCO network, we expect minor differences in the actual transmission curves and detector responses from telescope to telescope. Our DAWDs are expected to be much hotter than other stars in the FoV, so the consequent differences in the color response from one telescope to another can induce an excess variation to be seen for the DAWD stars, since the instrumental magnitudes from epoch to epoch were adjusted by matching their ensemble averages across the different exposures. In practice, this does appear as a large effect for observations obtained by one particular telescope at the Cerro Tololo Inter-American Observatory (observatory code LSC), identified as *lsc1m004* in the image header. The DoPHOT-based analysis described here clearly showed this discrepancy. Subsequently, measurements from this telescope were discarded from all final DoPHOT and DAOPHOT photometric catalogs. With this exclusion in place, the results from the different analysis methods are in general agreement, and lead to the star-by-star evaluations presented in Section 5.

We also used the final DAOPHOT photometric catalogs to calculate a reduced χ^2 for all the stars in the FoV. Figure 6 shows the χ^2 plotted versus instrumental magnitude for the FoV observed toward WD0554-165. The position of the DAWD on the diagram is shown with a red star. This plot shows that WD0554-165 has a larger χ^2 compared to most of the stars observed in the same field, assumed not to be variables. However, to establish this DAWD as not stable, a more detailed analysis is needed.

Therefore, a sample of $\approx$10–20 *stable* comparison stars was selected for each of the DAWD sets of observations. As a requirement, stable stars have a detection in every frame, a χ^2 index smaller than the median χ^2 of all stars in the FoV,
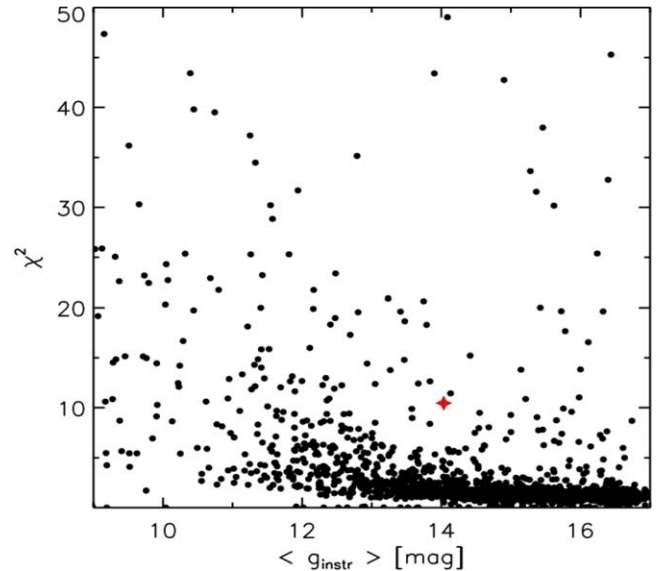
Figure 6. χ^2 index vs. instrumental average g magnitude for all stars observed in the FoV toward WD0554-165 (red star).

sharpness of the PSF in the range $-0.5 < \text{sharpness} < 0.5$ (to exclude extended objects and cosmic rays), and a proximity in instrumental g magnitude to the target DAWD within $\approx$0.2 mag.

An absolute calibration of the photometry was not performed as described in the previous section. However, we need to take into account spurious flux variations due to instrumental and atmospheric effects (observations are performed with different telescopes and detectors and from different sites in different conditions). The light curves of the selected stable stars are then compared to the light curves of the DAWD in the same FoV. The variation around the mean of the stable star magnitudes was averaged and the average 1σ dispersion was estimated. This dispersion is used as a variability threshold for the systematic observational and instrumental effects (see Figures 7, 8, and the figures in the Appendix).
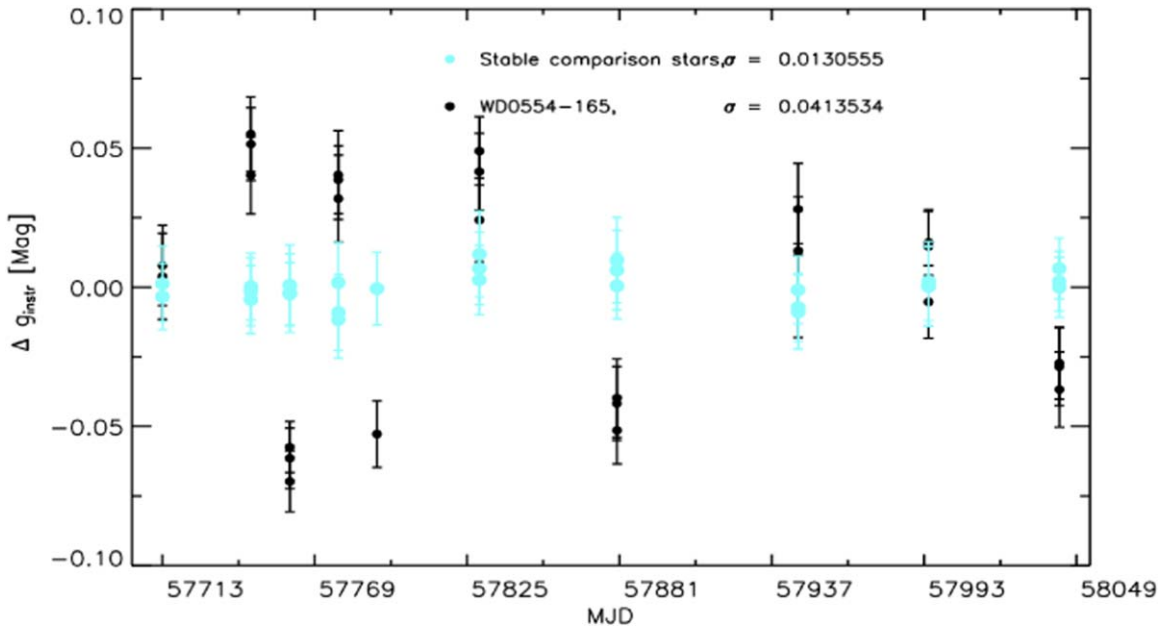
Figure 7. Single epoch minus the mean instrumental magnitude measurements for WD0554-165 as a function of observing epoch (black-filled dots). Averaged relative magnitudes for a set of stable stars of comparable instrumental magnitude in the same FoV are overplotted as cyan-filled dots. The 1σ dispersion of the measurements of the stable stars and the DAWD is labeled. Error bars are shown.

Figure 7 shows the single epoch minus the weighted mean instrumental magnitude as a function of the Mid Julian Date (MJD) for WD0554-165 (black-filled dots). Averaged magnitudes for a set of stable stars of comparable instrumental magnitude in the same FoV are also plotted as cyan-filled dots. The selected comparison stars have a χ^2 index of less than 1.2, while WD0554-165 has an index of 10.5. WD0554-165 shows clear signs of variability, with a measurement 1σ dispersion of $\sim$0.04 mag, four times larger compared to the stable star average dispersion of $\sigma \sim 0.01$ mag (Figure 7).

Figure 8 shows the light curve plot for WDFS2351+37: its χ^2 index is 1.0 and the dispersion of the measurement is $\sim$0.015 mag, of the same order as the measurement dispersion of the stable stars, $\sigma \sim 0.012$ mag. This DAWD was considered stable and included in our spectrophotometric standard network.

The light curve for SDSSJ203722.169-051302.964 (see Figure 30 in Appendix C), a candidate binary system from spectroscopic data, shows hints of variability with a χ^2 index of 3.8 and a dispersion of the measurements of $\sigma \sim 0.04$ mag, a factor of 2 larger than the comparison star average measurement dispersion, $\sigma \sim 0.02$ mag.

Stars SDSSJ203722.169-051302.964 and WD0554-165 were excluded from our network of spectrophotometric standard DAWDs due to their variable nature (see also the discussion in CA19 and NA19).

4.1. Alternative Variability Indices

To further refine our variability analysis we also used two other variability indices, namely the interquartile range (IQR) and the von Neumann ratio (η). These pair of indices proved to be very effective when working with data affected by outliers and different kinds of variability and periods (Sokolovsky et al. 2017), which is our case. However, these indices might be less effective when working with a limited set of measurements as the LCO data we have for our DAWDs.

The two indices are defined as:

1. the IQR is calculated as the difference between the median value of the upper and the lower half of the data points, by excluding the 25% higher and lower values:
2. and the von Neumann index is calculated as:

$$\eta = \frac{\frac{\sum_{i=1}^{N-1}(m_{i+1} - m_i)^2}{(n-1)}}{\frac{\sum_{i=1}^{N}(m_i - \bar{m})^2}{(n-1)}}. \qquad (2)$$

These variability indices were calculated for all the DAWDs, even those classified as *variable* with the χ^2 index and the comparison stars or excluded for other reasons, and for all the stars in the FoV. Figure 9 shows the difference between the IQR index and $1.34 \times \sigma$ (top panel), where σ is the dispersion of the measurements, and the $1/eta$ index (bottom, the larger $1/eta$ and the higher is the possibility that a star is variable) plotted versus the average instrumental magnitude (g) for the FoV observed toward WD0554-165. The position of the DAWD on the variability index plots is shown with a red star. The difference between the IQR index and $1.34 \times \sigma$ seems consistent with values of most stars in the same FoV, while the $1/eta$ index of WD0554-165 is $\sim$15, much higher compared to the average $1/eta$ index for the other observed stars in the field, assumed not to be variables, i.e., $\lesssim$2.

4.2. ATLAS Data

For a few DAWDs, the LCO light curves and the different variability indices were still inconclusive to classify them as fully stable stars. Therefore, we downloaded the Asteroid Terrestrial-impact Last Alert System (ATLAS; Heinze et al. 2018; Tonry et al. 2018) survey data, when available, for targets with decl. north of $-50°$. In particular, we downloaded forced photometry in the cyan (c) and orange (o) filters for 7 DAWDs in the Northern hemisphere and 4 in the Southern one.
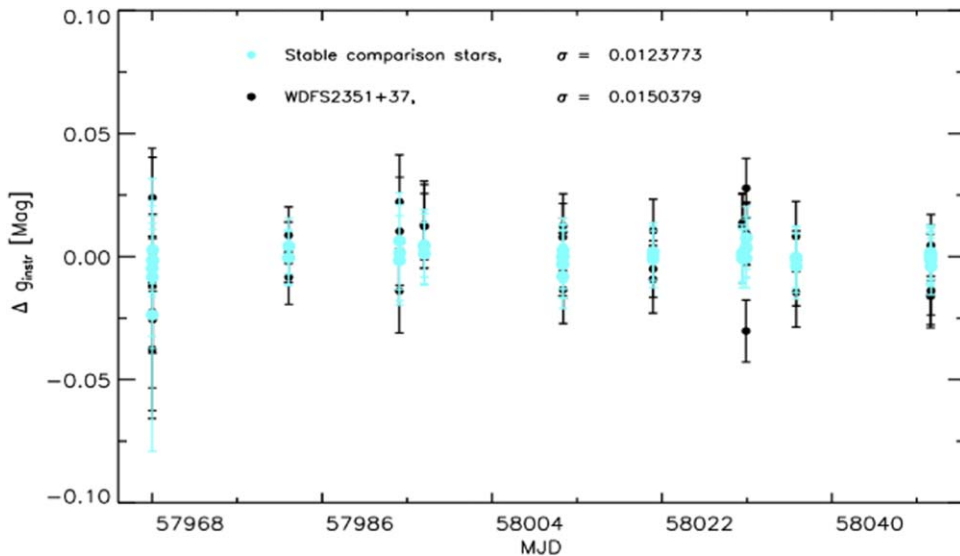
Figure 8. Same as Figure 7 but for WDFS2351+37.
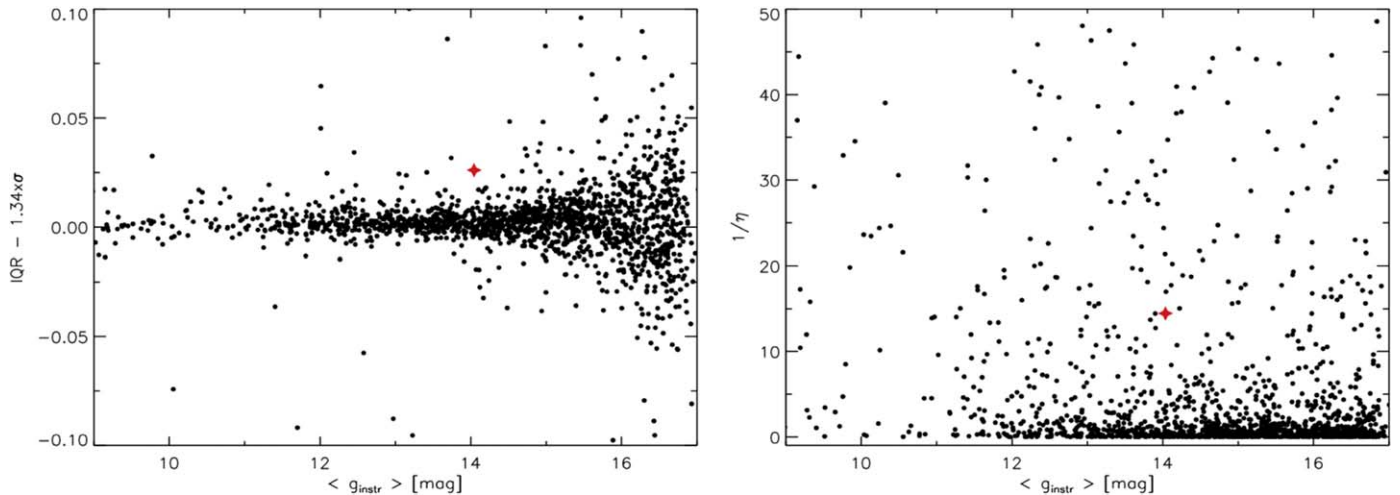
Figure 9. IQR index compared to 1.34 × σ (top panel) and 1/*eta* index (bottom) vs. the average *g* instrumental magnitudes for all the stars in the FoV observed toward WD0554-165. The DAWD is marked with a red star symbol.

We also retrieved ATLAS time-series photometry for a set of up to 100 stars with similar instrumental magnitudes as the DAWD ($-0.5 \lesssim m_{\mathrm{DAWD}} \lesssim +0.5$) in the LCO FoV. We then calculated the IQR and η variability indices for all the observed stars to be compared with the value of the DAWD. The two ATLAS variability indices are also listed in Table 4 when available. Figure 10 shows the IQR compared to 1.34 × σ and the 1/η index versus the ATLAS *cyan* magnitudes for star WDFS1314-03 and ≈100 stars of similar LCO instrumental *g* magnitude. Since we do not have the color information for stars in the LCO FoV, the selected comparison stars are generally brighter (and redder) than the DAWD in the ATLAS filters, as displayed in the figure. The top panel of Figure 10 shows that the IQR index for WDFS1314-03 is consistent with the dispersion of the measurements and with that of stars of similar LCO *g* instrumental magnitude, and the 1/η index (bottom panel) is similar to that of most stars in the FoV. WDFS1314-03 is found to be stable and kept in our network of standards. For more details about this DAWD please see Section 5.

4.3. TESS Data

We also matched our sample of DAWDs with the TESS archive and found data for 35 of them (WDFS0228-08, WDFS0815+07, and SDSSJ203722.169-051302.964 do not have available observations). All TESS data were reduced with the `TESSreduce` package, which produced flux-calibrated difference imaged light curves (Ridden-Harper et al. 2021). Since calibrating TESS data between sectors remains unreliable, for each sector we subtracted the median flux of the sector from the DAWD light curve. Although this process limits the effects of cross-sector calibration, it may flatten periods that last for longer than a sector (~27 days). We checked all the light curves for variability by using a Lomb–Scargle periodogram analysis. In the case of some DAWDs, the light curves contain residual flux from the periodic TESS scattered light background, and have issues with image alignment. DAWDs affected by these reduction artifacts contained periodic signals from the drift in image alignment and spikes in the background, substantially decreasing the S/N of the observations. For these

Table 4
Photometric Parameters for all the Observed DAWDs

Star	N_{exp}	G (mag)	σ_{LCO} (mag)	χ^2	IQR	$1/\eta$	IQR_{ATLAS}	$1/\eta_{ATLAS}$	IR Excess
				Northern and equatorial DAWDs					
WDFS0103-00[a]	39	19.301 ± 0.003	0.03	2.1	0.03	0.28	…	…	…
WDFS0228-08[a]	40	19.975 ± 0.006	0.04	2.2	0.06	0.39	…	…	…
WDFS0248+33	30	18.521 ± 0.002	0.03	1.5	0.03	0.11	…	…	…
WDFS0727+32	21	18.189 ± 0.002	0.01	0.7	0.02	0.51	…	…	…
WDFS0815+07	24	19.932 ± 0.005	0.03	1.0	0.05	0.60	…	…	…
WDFS1024-00	20	19.083 ± 0.003	0.02	0.7	0.03	0.60	…	…	…
WDFS1110-17[a]	36	18.048 ± 0.001	0.03	4.3	0.05	6.78	0.28	1.65	No
WDFS1111+39	17	18.644 ± 0.002	0.02	1.6	0.02	0.20	…	…	…
WDFS1206+02	24	18.850 ± 0.002	0.02	1.1	0.02	1.74	…	…	…
WDFS1214+45	6	17.979 ± 0.001	0.02	1.8	0.00	0.06	…	…	…
WDFS1302+10	9	17.239 ± 0.001	0.04	9.0	0.06	4.71	0.07	1.38	No
WDFS1314-03[a]	18	19.307 ± 0.003	0.02	0.7	0.04	0.23	0.28	0.13	…
WDFS1514+00[a]	28	15.884 ± 0.001	0.03	6.0	0.04	1.60	0.05	42.95	Upp. limit
WDFS1557+55	20	17.691 ± 0.001	0.02	1.3	0.03	4.09	…	…	…
WDFS1638+00[a]	12	19.025 ± 0.002	0.02	0.9	0.02	23.3	0.91	2.86	…
WDFS1814+78	18	16.745 ± 0.001	0.01	1.0	0.01	0.33	…	…	…
WDFS2101-05[a]	17	18.827 ± 0.002	0.02	2.9	0.02	0.99	0.29	77.25	Upp. limit
WDFS2329+00	26	18.292 ± 0.002	0.02	1.6	0.02	0.00	…	…	…
WDFS2351+37	40	18.235 ± 0.002	0.01	1.0	0.02	0.52	…	…	…
				Southern DAWDs					
WDFS0122-30	18	18.664 ± 0.001	0.03	2.3	0.03	1.42	…	…	…
WDFS0238-36[a]	17	18.236 ± 0.001	0.03	6.8	0.03	8.29	…	…	…
WDFS0458-56	32	17.959 ± 0.001	0.02	3.9	0.02	0.12	…	…	…
WDFS0541-19[a]	27	18.433 ± 0.002	0.03	3.2	0.03	0.09	0.18	33.01	…
WDFS0639-57	10	18.375 ± 0.002	0.02	3.2	0.03	33.00	…	…	…
WDFS0956-38	16	18.002 ± 0.001	0.02	3.1	0.04	0.14	…	…	…
WDFS1055-36[a]	14	18.196 ± 0.001	0.02	3.5	0.04	1.67	0.13	1.04	…
WDFS1206-27[a]	14	16.667 ± 0.001	0.02	7.7	0.02	0.73	0.07	16.68	No
WDFS1434-28[a]	21	18.103 ± 0.002	0.02	2.0	0.02	0.01	0.22	0.07	…
WDFS1535-77[a]	24	16.765 ± 0.001	0.02	1.9	0.12	1.30	…	…	No
WDFS1837-70	9	17.91 ± 0.001	0.02	1.3	0.01	11.72	…	…	…
WDFS1930-52	17	17.673 ± 0.001	0.03	11.0	0.04	0.66	…	…	Upp. limit
WDFS2317-29[a]	20	18.526 ± 0.002	0.03	5.0	0.05	0.20	…	…	…
				Discarded DAWDs					
SDSSJ041053.632-063027.580	38	18.990 ± 0.002	0.03	2.7	0.04	0.02	…	…	…
WD0554-165	27	17.944 ± 0.001	0.04	10.5	0.08	14.45	0.23	0.24	…
SDSSJ172135.97+294016.0	27	19.598 ± 0.003	0.04	1.4	0.06	0.13	…	…	…
SDSSJ203722.169-051302.964	15	19.110 ± 0.002	0.04	3.8	0.02	0.06	…	…	…
WD0418-534	45	16.420 ± 0.001	0.03	16.4	0.04	2.98	…	…	Upp. limit
WD0757-606	11	18.953 ± 0.002	0.02	1.0	0.03	0.02	…	…	…

Notes. Magnitudes with errors are from Gaia EDR3 (G), and the dispersion of the measurements is from the LCO time-series (σ_{LCO}).
[a] We warn the users that these standard star measurements could be affected by the presence of close red faint neighbors when observed from the ground.

(This table is available in machine-readable form.)

targets, it is difficult to definitively assess the absence or presence of variability.

TESS data for the DAWDs span both the primary and extended missions, which have cadences of 30 and 10 minutes, respectively. For consistency, we binned the light curves to a cadence of 30 minutes and 1 hr to increase the S/N. Analysis of this data does not show any significant sign of variability, or any peculiarities in the DAWD light curves. However, at the wavelength of the TESS filter ($\lambda \sim 8000$ Å) and due to the instrument's low spatial resolution ($21''$ per pixel), the light curves of the DAWDs might be contaminated by faint red neighbor stars. For more details on neighbor star contamination,

see the discussion in Section 5 and the NIR image cutouts in Appendix C.

4.4. PS1 and ZTF Data

We matched almost all northern and equatorial DAWDs with Pan-STARRS1 (PS1) data release 2[25] (Magnier et al. 2020) and ZTF data release 8[26] (Bellm et al. 2019) single epoch detection archives, except for WDFS1557+55. All ZTF matches have

---

[25] https://catalogs.mast.stsci.edu/panstarrs/
[26] We used the SNAD ZTF viewer for ZTF data (Malanchev et al. 2021) https://ztf.snad.space.
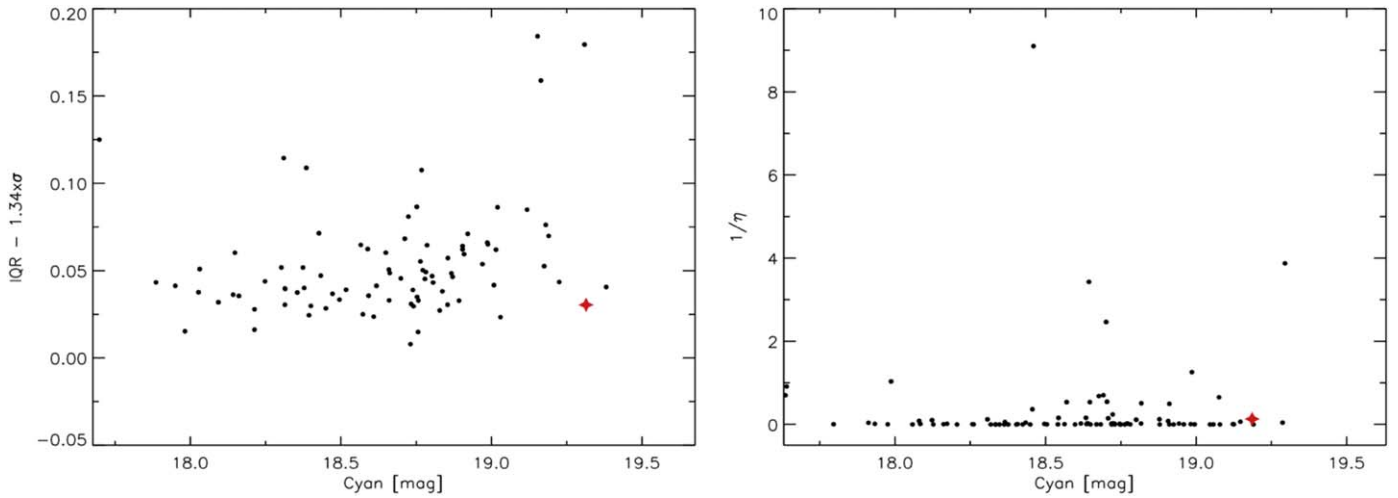
Figure 10. IQR index compared to $1.34 \times \sigma$ (top panel) and $1/eta$ index (bottom) vs. *cyan* average magnitudes from the ATLAS survey for WDFS1314-03 (red star symbol) and ≈ 100 stars of similar LCO instrumental *g* magnitude in the same FoV.

observations in the *g* and *R* filters, with most of the single filter light curves of the DAWDs having a modified χ^2 index below ~ 3.3. The only exception is the *r*-band light curve for WDFS0815+07, with a χ^2 index value of 5.9 due to a single bright outlier measurement. Most of the PS1 matches have observations in all five filters, *g*, *r*, *i*, *z*, and *y*, while the faint stars WDFS0103-00, WDFS0228-08, and WDFS0815+07, do not have any measurements in *y*. Almost all light curves have modified χ^2 index below ~ 6.1. The two exceptions are the *z*-band light curve of SDSSJ041053.632-063027.580, which shows a faint outlier observation making the index 36.7, and the brightest DAWD, WDFS1514+00, with $\chi^2 = 18.3$ for the *g* band and 7.3 for the *r* band, possibly caused by an underestimate of the measurement uncertainties.

4.5. NIR Excess

For some of the brightest DAWDs that showed hints of variability based on some indices in near-infrared (NIR) photometry from PS1, UKIRT, DENISE, VISTA, and Wide-field Infrared Survey Explorer (WISE) were available and we downloaded it from the VOSA (Virtual Observatory SED Analyzer) database[27] (Bayo et al. 2008, see Table 4). For four stars, two in the Northern hemisphere (WDFS1110-17, WDFS1302+10) and two in the Southern (WDFS1206-2, WDFS1535-77), no clear NIR excess was identified. However, for the other four DAWDs, two in the Northern hemisphere (WDFS1514+00, WDFS2101-05) and two in the Southern (WD0418-534, WDFS1930-52), an upper limit to the NIR excess was identified from WISE photometry. Figure 11 shows the SED for star WDFS1514+00 with data from the ultraviolet to the NIR retrieved from VOSA (GALEX, SDSS, APASS, Gaia, DECam, PS1, DENIS, UKIRT, Two Micron All Sky Survey (2MASS), WISE). The three last points are WISE upper limit measurements. Therefore, it is not possible to confirm the presence of NIR excess for this DAWD nor to fully exclude it. The star is kept as part of our spectrophotometric standard and users should be aware of the possibility of NIR excess that could contaminate its measurements. However, the HST SED for this star does not show any indication of a NIR excess (NA19). For more details on neighbor star contamination for

---

27 http://svo2.cab.inta-csic.es/theory/vosa/index.php

this DAWD please see the discussion in Section 5 and the NIR image cutouts in the Appendix C.

Seven of these eight DAWDs were included in our set of spectrophotometric standards with the caveat that photometric measurements from ground-based observatories could be affected by the presence of red faint neighbors. WD0418-534 was excluded due to its potential variability and the presence of infrared excess (for more details about these eight DAWDs please see Section 5 and Table 4).

5. Description of Findings for Each DAWD

In the following, we describe the results for the 38 DAWDs observed with LCO. All the light curves are shown in Appendix A and B. In the same section, we provide finding charts for all the stars based on WFC3/HST F160W images. Table 4 summarizes the results of the LCO time-spaced data analysis and lists parameters for the 32 established spectro-photometric standard DAWDs. The discarded DAWDs are listed at the bottom of the same table. The distribution on the sky of the final network of 32 standards is shown in the Hammer–Aitoff projection in Figure 1.

5.1. Northern and Equatorial DAWDs

1. *WDFS0103-00* The light curve of this star does not show signs of variability (see Figure 12 in Appendix A). The χ^2 index is 2.1 and the dispersion of the LCO photometric measurements is $\sigma \sim 0.03$ mag (see Table 4, where the values χ^2 are also listed), compared to the stable star dispersion of $\sigma \sim 0.02$ mag. The WFC3 F160W image for this star (see Figure 48 in Appendix C) shows a neighbor faint red source at $\sim 5''$ that could contaminate the LCO photometry. WDFS0103-00 is classified as a stable WD by Kleinman et al. (2013). On the basis of this evidence, we keep this DAWD in our sample of standard stars and warn the users about the close-by faint red star when observing from ground-based observatories.

2. *WDFS0228-08* The light curve of this star shows some hints of variability (Figure 13). The χ^2 index is 2.2, and the dispersion of the LCO measurements is $\sigma \sim 0.04$ mag, compared to the stable star average dispersion of
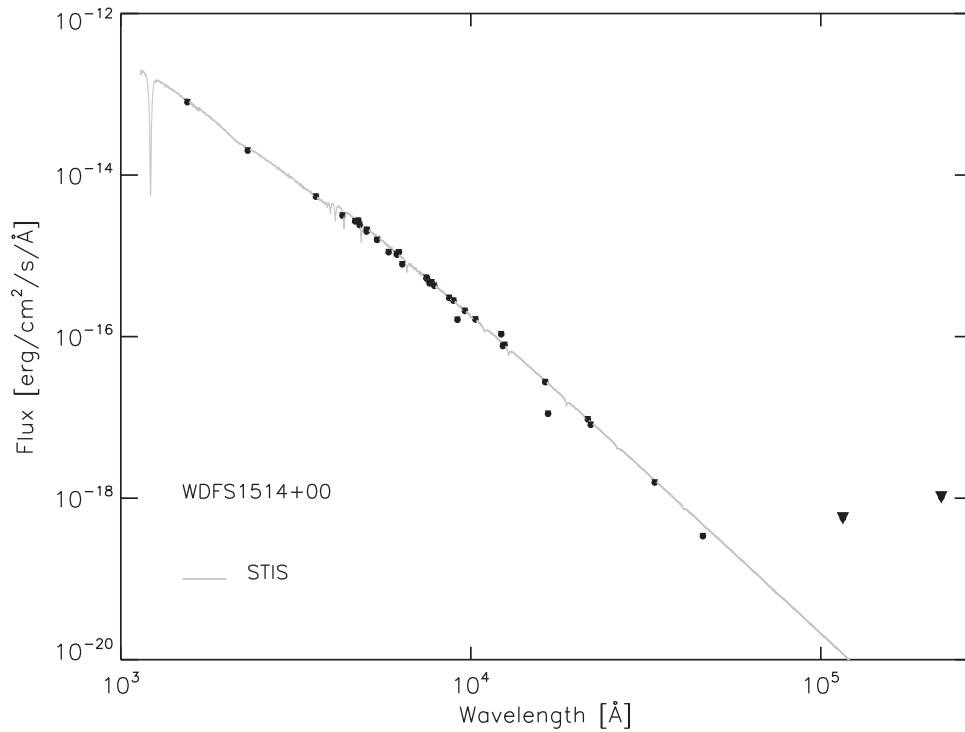
Figure 11. CALSPEC STIS spectrum of WDFS1514+00 (gray solid line) with overplotted photometric observations from GALEX, SDSS, APASS, Gaia, DECam, PS1, DENIS, UKIRT, 2MASS (black-filled dots). The WISE upper limit measurements are marked with downward-filled triangles.

$\sigma \sim 0.03$ mag. The WFC3 F160W image (Figure 48) shows a faint red source at $\sim 1''$ distance. The source is not visible in the F775W images and in the bluer WFC3-UVIS filters but could contaminate the LCO photometry. We do not exclude this DAWD from our sample of standards but we warn the users when observing this star from ground-based observatories due to the very close-by red source.

3. *WDFS0248+33* The light curve of this star does not show clear signs of variability (Figure 14). The χ^2 index is 1.5, with a dispersion of the measurements of $\sigma \sim 0.04$ mag, compared to the stable star dispersion of $\sigma \sim 0.03$ mag. This DAWD is included in our sample of standard stars. However, we caution the user about the high estimated reddening toward this star, i.e., $A_V \sim 0.30$ mag.

4. *SDSSJ041053.632-063027.580* The light curve of this star shows a few hints of variability (Figure 15). The χ^2 index is 2.7, with a dispersion of the measurements of $\sigma \sim 0.03$ mag compared to the stable star average dispersion of $\sigma \sim 0.02$ mag. The WFC3 F160W image shows the presence of a few faint red sources at distances in the range $4''$–$6''$, and 4 luminous galaxies at about $10''$ distance (Figure 48). The galaxies are also visible in the WFC3-UVIS F775W images, but not in WFC3-UVIS images collected in bluer filters. This star was classified as a DA:ME from Kleinman et al. (2013), i.e., it has a faint M-dwarf companion. We then exclude this DAWD from our sample of standard stars (see also NA19).

5. *WD0554-165* This star has already been discussed above and the light curve is shown in Figure 7. We exclude it from our sample of standard stars.

6. *WDFS0727+32* The light curve of this star does not show any sign of variability, with a χ^2 index of 0.7 and a dispersion of the measurements of $\sigma \sim 0.01$ mag

compared to the stable star dispersion of $\sigma \sim 0.01$ mag. This DAWD is included in our network of standard stars (Figure 16).

7. *WDFS0815+07* The light curve of this star does not show signs of variability, with a χ^2 index of 1.0. However, the LCO photometry seems quite noisy, with a dispersion of the measurements of $\sigma \sim 0.03$ mag, smaller compared to the average dispersion of the selected stable stars, $\sigma \sim 0.04$ mag (Figure 17). This DAWD is included in our network of standard stars.

8. *WDFS1024-00* The light curve of this star does not show signs of variability, with a χ^2 index of 0.7 and a dispersion of the measurements of $\sigma \sim 0.02$ mag, comparable to the average dispersion of the selected stable stars, $\sigma \sim 0.02$ mag (Figure 18). We keep this DAWD in our network of standard stars.

9. *WDFS1110-17*: The light curve of this star shows some hints of variability. The χ^2 index is 4.3, with a dispersion of the measurements of $\sigma \sim 0.03$ mag, three times larger than the stable star average dispersion of $\sigma \sim 0.01$ mag (Figure 19). However, the IQR index from LCO and ATLAS photometry is low, 0.05 and 0.28, respectively, and comparable to the measurement dispersion and to the IQR index of all other stars in the FoV. The inverse of the von Neumann index based on LCO photometry is high, ~ 7, possibly due to the small number of measurements available (36). On the other hand, the inverse of the von Neumann index based on ATLAS photometry is 1.65, comparable to that of the other stars in the field. Furthermore, TESS, PS1, and ZTF do not show this DAWD as variable, and there is no evidence of IR excess. However, the WFC3 F160W image shows the presence of a few faint red sources at $\sim 2''$, $3''$, and $3''.5$ that could contaminate the LCO photometry (Figure 48). Therefore,

16

we do not exclude this DAWD from our sample of standards but we warn the users when observing the star from ground-based observatories due to the close-by red sources.

10. *WDFS1111+39:* The light curve of this star does not show any sign of variability, with a χ^2 index of 1.6 and a dispersion of the measurements of $\sigma \sim 0.02$ mag, slightly larger than the stable star dispersion $\sigma \sim 0.01$ mag (Figure 20). This DAWD is included in our sample of standard stars.

11. *WDFS1206+02* The light curve of this star does not show signs of variability with χ^2 index of 1.1 and a dispersion of the measurements of $\sigma \sim 0.02$ mag, comparable to the stable star dispersion $\sigma \sim 0.02$ mag (Figure 21). This DAWD is included in our sample of standard stars.

12. *WDFS1214+45* The light curve of this star does not show any sign of variability, with a χ^2 index of 1.8 and a dispersion of the measurements of $\sigma \sim 0.02$ mag, comparable to the stable star dispersion $\sigma \sim 0.02$ mag (Figure 22). This DAWD is included in our sample of standard stars.

13. *WDFS1302+10* The light curve of this star shows a few hints of variability, with $\chi^2 = 9.0$ and a dispersion of the measurements $\sigma \sim 0.04$ mag, compared to the stable star dispersion, $\sigma \sim 0.02$ mag (Figure 23). The IQR index based on LCO and ATLAS photometry is 0.06 and 0.07, respectively, and comparable to the measurement dispersion. The $1/\eta$ index from the same data sets is ~ 5 and 1.38, respectively. The relatively high von Neumann index based on LCO data might be due to the low (9) number of measurements available. TESS, PS1, and ZTF do not show this DAWD as variable, and there is no evidence of IR excess. Also, the WFC3 F160W image does not show the presence of close-by red sources (Figure 48). Concluding, we keep this DAWD in our network of standard stars.

14. *WDFS1314-03* The light curve of this star does not show signs of variability, with $\chi^2 = 0.7$ and a dispersion of the measurements of $\sigma \sim 0.02$ mag, comparable to the stable star dispersion, $\sigma \sim 0.02$ mag (Figure 24). The IQR and the $1/\eta$ index based on LCO and ATLAS data are also small. However, the WFC3 F160W image shows the presence of faint red neighbor at $\sim 0''.8$, $1''$, and $3''$ that could contaminate the LCO photometry (Figure 48). Therefore, we do not exclude this DAWD from our sample of standards but we warn the users when observing this star from ground-based observatories due to the close-by red sources.

15. *WDFS1514+00* The light curve of this star shows some level of variability, with a dispersion of the measurements of $\sigma \sim 0.03$ mag compared to the stable star dispersion of $\sigma \sim 0.01$ mag and a χ^2 index of 6.0 (Figure 25). On the other hand, the IQR index based on LCO and ATLAS photometry is low, 0.04 and 0.05, respectively, and comparable to the measurement dispersion. The $1/\eta$ based on these two data sets is ~ 1.7 and 43, but it could be due to the low number of measurements available from LCO and contamination by neighbors in the ATLAS survey. The WFC3 F160W image shows indeed the presence of faint red neighbors at $\sim 3''$ and $4''.5$ that could contaminate the photometry and there is a hint of the presence of some IR excess, possibly due to the

contamination (Figure 48). TESS, PS1, and ZTF do not show this DAWD as variable, and on the basis of all the evidence, we do not exclude this star from our network of standards. However, we caution observers when using this DAWD from ground-based observatories due to the close-by red sources.

16. *WDFS1557+55* The light curve of this star does not show signs of variability, with a χ^2 index of 1.3 and a dispersion of the measurements of $\sigma \sim 0.02$ mag comparable to the stable star dispersion $\sigma \sim 0.02$ mag (Figure 26). This DAWD is included in our network of standard stars.

17. *WDFS1638+00* The light curve of this star does not show signs of variability, with a χ^2 index of 0.9 and a dispersion of the measurements of $\sigma \sim 0.02$ mag as the stable star dispersion of $\sigma \sim 0.02$ mag (Figure 27). However, the WFC3 F160W image shows the presence of faint red neighbors at $\sim 3''$ and $4''$ that could contaminate LCO photometry (Figure 49). These red sources are also visible in the F775W images, but disappear in the WFC3-UVIS bluer filter images. This DAWD is not excluded from our network of standards. However, we warn observers when using this star from ground-based observatories due to the close-by red sources.

18. *SDSSJ172135.97+294016.0* The light curve of this star is quite noisy with a dispersion of the measurements of $\sigma \sim 0.04$ mag, slightly larger than the stable star dispersion $\sigma \sim 0.03$ mag, and $\chi^2 = 1.4$ (Figure 28). This DAWD is excluded from our network of standard stars as a result of its lower $T_{\rm eff}$ (for more information see NA19).

19. *WDFS1814+78* The light curve of this star does not show any sign of variability, with a $\chi^2 = 1.0$, and a dispersion of the measurements of $\sigma \sim 0.01$ mag, comparable to the stable star dispersion $\sigma \sim 0.01$ mag (Figure 29). This DAWD is included in our network of standard stars.

20. *SDSSJ203722.169-051302.964* This star has already been discussed above and the light curve is shown in the Appendix in Figure 30. We exclude this DAWD from our sample of standard stars due to its binary nature.

21. *WDFS2101-05* The light curve of this star shows some level of variability, and a χ^2 index of 2.9 (Figure 31). However, the dispersion of the measurements is $\sigma \sim 0.02$ mag, slightly larger compared to the stable star dispersion of $\sigma \sim 0.01$ mag, and the IQR and $1/\eta$ indices have low values comparable to the other stars in the FoV. The $1/\eta$ index calculated from ATLAS data is very high, but this photometry could be contaminated by neighbor stars. The WFC3 F160W image shows indeed the presence of faint red neighbors at $\sim 2''$ and $5''$ that could contaminate LCO and ATLAS photometry (Figure 49). One of the sources is also visible in the WFC3-UVIS F775W images. This DAWD is not excluded from our network of standards. However, we caution observers when using this star from ground-based observatories due to the close-by red sources.

22. *WDFS2329+00* The light curve of this star does not show clear signs of variability. The χ^2 index is 1.6 and the dispersion of the measurements of $\sigma \sim 0.02$ mag, is the same as the stable star dispersion $\sigma \sim 0.02$ mag (Figure 32). Moreover, the IQR and the $1/\eta$ indices do not highlight any peculiarities for this star. On the basis of this evidence, we keep this DAWD in our sample of standard stars.

23. *WDFS2351+37* This DAWD has already been discussed above and the light curve is shown in Figure 8, and it is included in our sample of standards.

5.2. Southern DAWDs

1. *WDFS0122-30* The light curve of this star shows some level of variability, with a χ^2 index of 2.3 (Figure 33). However, the dispersion of the measurements of $\sigma \sim 0.03$ mag, is only slightly larger compared to the stable star dispersion $\sigma \sim 0.02$ mag. Moreover, the IQR and the $1/\eta$ indices do not highlight any peculiarities for this star. This DAWD is included in our network of standard stars.

2. *WDFS0238-36* The light curve of this star shows hints of variability, with a χ^2 index of 6.8 and a dispersion of the measurements of $\sigma \sim 0.03$ mag compared to the stable star dispersion $\sigma \sim 0.01$ mag (Figure 34). The IQR index is comparable to the measurement uncertainties, but the $1/\eta$ index is high compared to the other stars in the FoV. However, this could be due to the small number of LCO measurements (17). TESS, PS1, and ZTF do not show this DAWD as variable. However, the WFC3 F160W images show the presence of a faint red source at $\sim 8''$, also visible in the WFC3 F775W images, that may contaminate the LCO photometry, since the quality of observing nights for this star were not very good (see also Table 4). Therefore, we keep this DAWD in our network of standards, but warn the users when observing this star from ground-based observatories due to the close-by red sources.

3. *WD0418-534* The light curve of this star shows signs of variability, with a χ^2 index of 16.4 and a dispersion of the measurements of $\sigma \sim 0.03$ mag compared to the stable star dispersion $\sigma \sim 0.01$ mag (Figure 35). The IQR index is compatible with the measurement uncertainties, but the $1/\eta$ index is slightly higher compared to the other stars in the FoV. Unfortunately, no ATLAS data are available for this DAWD. TESS, PS1, and ZTF do not show this star as variable. However, the stars might show some infrared excess, which could be due to an unseen close-by red source. In light of this evidence, we decided to exclude this DAWS from our network of standards.

4. *WDFS0458-56* The light curve of this star shows hints of variability. The χ^2 index is 3.9 but the dispersion of the measurements is $\sigma \sim 0.02$ mag, slightly larger than the stable star dispersion $\sigma \sim 0.01$ mag (Figure 36). The IQR and $1/\eta$ indices are comparable to those of the other stars in the FoV. TESS, PS1, and ZTF do not show this star as variable. On the basis of this evidence, we keep this DAWD in our sample of standard stars.

5. *WDFS0541-19* The light curve of this star shows hints of variability. The χ^2 index is 3.2 but the dispersion of the measurements is $\sigma \sim 0.03$ mag, slightly larger than the stable star dispersion $\sigma \sim 0.02$ mag (Figure 37). The IQR and $1/\eta$ indices are comparable to those of the other stars in the FoV, and TESS, PS1, and ZTF do not show this star as variable. However, $1/\eta$ calculated from ATLAS photometry is relatively high (33) but this could be due to contamination of the photometry from neighbor stars. The WFC3 *F*160w images show a very bright galaxy at $\sim 8''$ and a bright star at $\sim 12''$ that could contaminate ground-based photometry (Figure 50). Therefore, we

keep this DAWD in our network of standard stars. However, we warn observers when using this star from ground-based observatories due to the close-by bright red sources.

6. *WDFS0639-57* The light curve of this star shows hints of variability, with a χ^2 index of 3.2 (Figure 38). However, the dispersion of the measurements is $\sigma \sim 0.02$ mag, slightly larger compared to the stable star dispersion $\sigma \sim 0.01$ mag. The $1/\eta$ index for this star is quite high (33) compared to that of other stars in the FoV, but this is possibly due to the very low number of LCO measurements (10). TESS, PS1, and ZTF do not show this star as variable. On the basis of this evidence, we keep this DAWD in our network of standards.

7. *WD0757-606* The light curve of this star does not show any sign of variability, with a χ^2 index of 1.0 and a dispersion of the measurements of $\sigma \sim 0.02$ mag, comparable to the stable star dispersion $\sigma \sim 0.02$ mag (Figure 39). However, this DAWD is in an open cluster, NGC 2516, $\approx 40''$ from a very bright Be star (CD-60 1953), $G \approx 9$ mag, so its flux could be largely contaminated by the neighbor. Also, this star lies very close to the PSF area of an unidentified Rosat PSPC X-ray source (Chu et al. 2004). This DAWD is then excluded from our network of standards.

8. *WDFS0956-38* The light curve of this star does not show clear signs of variability. The χ^2 index is 3.1 but the dispersion of the measurements is $\sigma \sim 0.02$ mag, slightly larger compared to the stable star dispersion $\sigma \sim 0.01$ mag (Figure 40). Also, IQR and $1/\eta$ indices are comparable to those of the other stars in the FoV, and TESS, PS1, and ZTF do not show this star as variable. Therefore, we keep this DAWD in our sample of standard stars.

9. *WDFS1055-36* The light curve of this star shows a few signs of variability, with a χ^2 index of 3.5. However, the dispersion of the measurements is $\sigma \sim 0.02$ mag, slightly larger compared to the stable star dispersion $\sigma \sim 0.01$ mag (Figure 41). The IQR and $1/\eta$ indices from LCO and ATLAS photometry are comparable to those of the other stars in the FoV, and TESS, PS1, and ZTF do not show this star as variable. However, the WFC3 F160W images show the presence of faint red neighbors at $\sim 2''$, $3''$ and $4''$ that could contaminate LCO photometry (Figure 50). Therefore, we keep this DAWD in our network of standard stars. However, we warn observers when using this star from ground-based observatories due to the close-by red sources.

10. *WDFS1206-27* The light curve of this star shows some level of variability, with a χ^2 index of 7.7 and a dispersion of the measurements of $\sigma \sim 0.02$ mag, more than 3 times larger than the stable star dispersion $\sigma \sim 0.005$ mag (Figure 42). However, IQR and $1/\eta$ indices are comparable to those of the other stars in the FoV. The $1/\eta$ calculated from ATLAS data is high compared to the values of stars in the field, but this could be due to neighbors contaminating the DAWD photometry. The WFC3 F160W images show indeed the presence of a faint red source at $\sim 5''$, also visible in the WFC3 F775W images, that could contaminate the LCO and ATLAS photometry (Figure 50). However, no infrared excess seems to be present. TESS, PS1, and

ZTF do not show this star as variable. On the basis of this evidence, we keep this DAWD in our network of standards, and warn the users when observing this star from ground-based observatories due to the close-by red sources.

11. *WDFS1434-28* The light curve of this star does not show signs of variability, with a χ^2 index of 2.0, and a dispersion of the measurements of $\sigma \sim 0.02$ mag, compared to the stable star dispersion of $\sigma \sim 0.01$ mag (Figure 43). The IQR and $1/\eta$ indices based on LCO and ATLAS data are also comparable to those of the other stars in the FoV. The WFC3 F160W images show the presence of bright galaxies at $\sim 5''$ and $12''$ (Figure 50), also visible in the WFC3 F775W images, that could contaminate ground-based photometry. Therefore, we include this DAWD in our network of standards and warn the users when observing this star from ground-based observatories due to the close-by bright sources.

12. *WDFS1535-77* The light curve of this star does not show signs of variability, with a χ^2 index of 1.9, and a dispersion of the measurements of $\sigma \sim 0.01$ mag, comparable to the stable star dispersion $\sigma \sim 0.01$ mag (Figure 44). The WFC3 F160W images show the presence of a faint red source at about $5''$, also visible in the WFC3 F775W images, that could contaminate the LCO photometry (Figure 50). However, no infrared excess seems to be present. Therefore, we keep this DAWD in our network of standards and warn the users when observing this star from ground-based observatories due to the close-by red sources.

13. *WDFS1837-70* The light curve of this star does not show any signs of variability, with a χ^2 index of 1.3 and a dispersion of the measurements of $\sigma \sim 0.02$ mag comparable to the stable star dispersion $\sigma \sim 0.02$ mag (Figure 45). This DAWD is included in our network of standard stars.

14. *WDFS1930-52* The light curve of this star shows some level of variability, with a χ^2 index of 11.0 and a dispersion of the measurements of $\sigma \sim 0.03$ mag, three times larger than the stable star dispersion $\sigma \sim 0.01$ mag (Figure 46). However, the IQR and $1/\eta$ indices are comparable to those of the other stars in the FoV. Unfortunately, no ATLAS data are available for this star but TESS, PS1, and ZTF do not show variability. There is an upper limit for the infrared excess of this star, but there are no identified faint red neighbors in the WFC3 F160W image. We then keep this DAWD in our network of standards (Figure 50).

15. *WDFS2317-29* The light curve of this star shows some level of variability, with a χ^2 index of 5.0 and a dispersion of the measurements of $\sigma \sim 0.03$ mag, three times larger compared to the stable star dispersion $\sigma \sim 0.01$ mag (Figure 47). However, the IQR and $1/\eta$ indices are comparable to those of the other stars in the FoV. Unfortunately, no ATLAS data are available for this star but TESS, PS1, and ZTF do not show variability. The WFC3 F160W image does show the presence of very faint red objects at $\sim 2''$, $3''$ and $5''$ that could be contaminated LCO photometry (Figure 50). This DAWD is then included in our network of standard stars with a warning to the users if observing it from the ground.

6. Summary and Conclusions

In this manuscript, we presented a photometric analysis to investigate the stability of a set of 38 DAWDs, out of which 32 were established as spectrophotometric standards. The summary of the variability analysis and the list of the selected standards is presented in Table 4. Their distribution on the sky is shown in Figure 1.

All 38 DAWDs in our set have HST WFC3-UVIS and IR photometry, ground-based spectroscopy and LCO time-spaced data. HST photometric and spectroscopic data for 23 DAWDs distributed in the Northern hemisphere and around the celestial equators, and the reduction methods, were described in CA19. Final averaged and calibrated magnitudes on the HST photometric system, and $T_{\rm eff}$ and $\log g$ for these 23 Northern DAWDs, were provided in that work.

Spectra of 48 candidate WDs in the Southern hemisphere were analyzed here and 15 stars were selected as DAWDs, while the others were discarded for being DC WDs, DB degenerates, peculiar or magnetized WDs. The selected 15 DAWDs were observed with WFC3/HST and the photometry for these stars, as well as the methods used to derive the $T_{\rm eff}$ and $\log g$ parameters, will be illustrated in T. Axelrod et al. 2022, in preparation.

Time-spaced observations in the g band were collected with the LCO network of telescopes for all 38 DAWDs during 6 semesters between 2016 and 2018. Our cadence implied observing each star at least three times per night for a few nights in a row and then repeating the same observations monthly during the semester. The observations could not always be collected due to weather and condition restrictions, so cadence varied according to the target. Data were pre-reduced with the LCO Banzai pipeline, while PSF photometry was performed by using a custom-made photometric pipeline that integrates Python with DAOPHOTIV/ALLSTAR and ALLFRAME. We derived photometric catalogs with average magnitudes and light curves for all stars identified in the FoV ($\approx 26' \times 26'$) including the DAWDs. Note that no absolute calibration was performed since the goal of this analysis was to investigate the sample of candidate spectrophotometric standards for the presence of variability. However, light curves were corrected for differences in the observing conditions due to the usage of different detectors (the Sinistro cameras), different telescopes, and different observatories. Also, light curves were corrected for differences due to the observing conditions, such as seeing, cloud cover, and due to the different PSF used in the fits.

Photometry was also performed on the same data set with DoPhot. This analysis allowed us to identify a color effect in the DAWD observations collected with the LCO telescope "lmsc004" on the Cerro Tololo observing site. The measurements obtained from images collected with this telescope were excluded from the light curves of all the DAWDs.

Time-spaced photometry was analyzed by using several different variability indices, namely, a reduced χ^2, the von Neumann (η) index, and the IQR index. These indices provided very similar results for most stars.

Moreover, for each target and FoV we selected a sample of stable stars, approximately in the same magnitude range of the DAWD, measured in all the available images, with a good quality PSF fit and *shape* parameter, and low χ^2. The average dispersion of the measurements for the stable stars is used as a threshold to help establish the variability of the DAWD.

Calamida et al.

We also downloaded and used ATLAS time-series photometry in the cyan bandpass when available, i.e., for stars with decl. larger than $-50°$. We calculated the IQR and η indices for all stars in the LCO FoV based on ATLAS photometry and used the indices for the DAWDs to help determine their stability.

TESS, PS1, and ZTF light curves for some of the DAWDs were also analyzed when available, and did not show any of the stars being variable. However, the low spatial resolution of these surveys and the redder filters used in some of the observations, limit the validity of these data sets for this kind of analysis.

We verified the presence of IR excess by using WISE photometry available from the Virtual Observatory database for a few of the stars, and obtained upper limits for four DAWDs, out of which one star was excluded from our network, mainly on the basis of the variability detected from the LCO light curve.

In summary, two of the Northern DAWDs, namely SDSSJ203722.169-051302.964 and WD0554-1656, were excluded for the variability detected in their LCO light curves and, in the case of SDSSJ203722.169-051302.964 in the spectra, as also described in CA19 and NA19.

We then excluded SDSSJ172135.97+294016.0, due to its T_{eff} being lower than 20,000 K, which is the low-temperature limit established to select our candidate standard DAWDs, and SDSSJ041053.632-063027.580, classified as a binary with an M-dwarf companion by Kleinman et al. (2013).

From the Southern hemisphere sample of DAWDs, WD0418-534 and WD0757-606 were excluded due to detected variability in the LCO light curves, and in the case of WD0757-606 also for the proximity of a very bright Be star that could contaminate the ground-based and space observations.

The final list of established spectrophotometric standards includes 32 stars listed in Table 4 of this manuscript and their new names (WDFSXXXX-XX), Gaia DR3 coordinates, and PMs are listed in Table 1. At the end of Table 4, the discarded DAWDs are also listed. These were not assigned a new name. Figure 1 shows a Hammer–Aitoff projection of the sky with the distribution of the 32 established spectrophotometric standards. These are distributed homogeneously on the sky so that at least two of them would be available to be observed from any observatory on the ground at any time at airmass less than two.

Finding charts with positions and Gaia magnitudes for all the DAWDs are in Appendix C.

Appendix A
Northern DAWD Light Curves

The light curves for all the 23 DAWDs in the Northern hemisphere and around the celestial equators are shown in Figures 12–32. Plots are listed in order of increasing R.A.
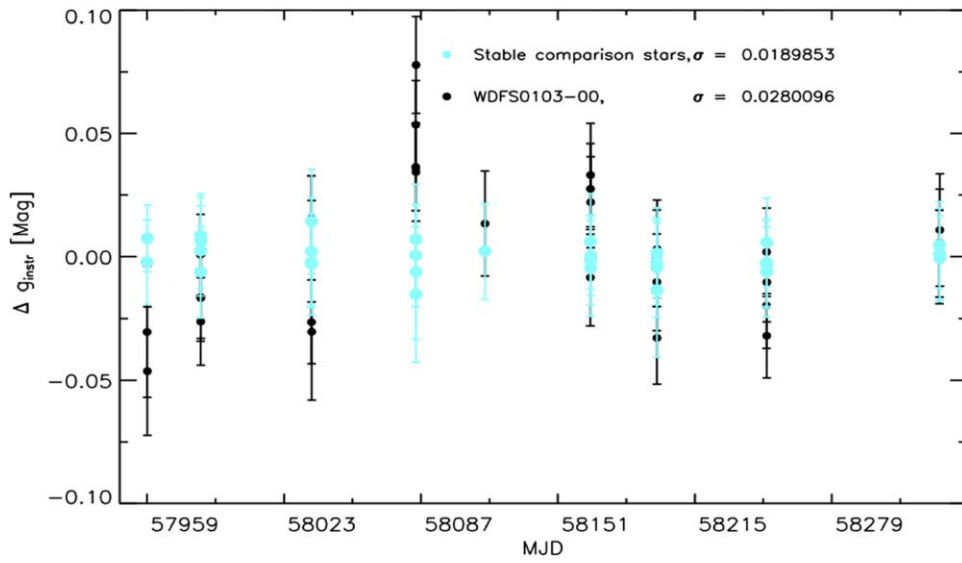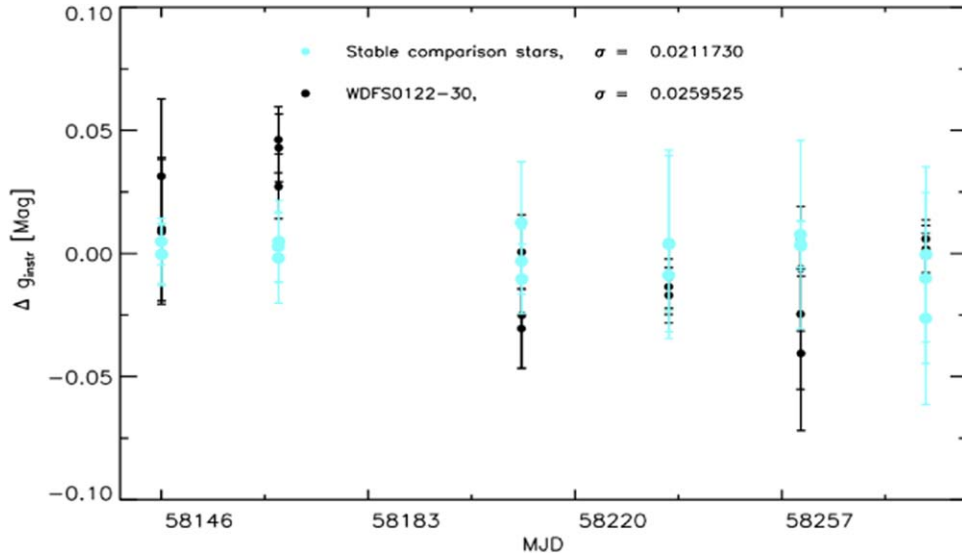
Figure 12. Single epoch minus the mean instrumental magnitude measurements for the Northern DAWD WDFS0103-00 as a function of observing epoch (black crosses). Averaged and binned relative magnitudes for a set of stable stars of comparable instrumental magnitude in the same FoV are overplotted as a red-shaded area. The variability index of the selected stars and the measurement dispersion are listed. Error bars are shown.
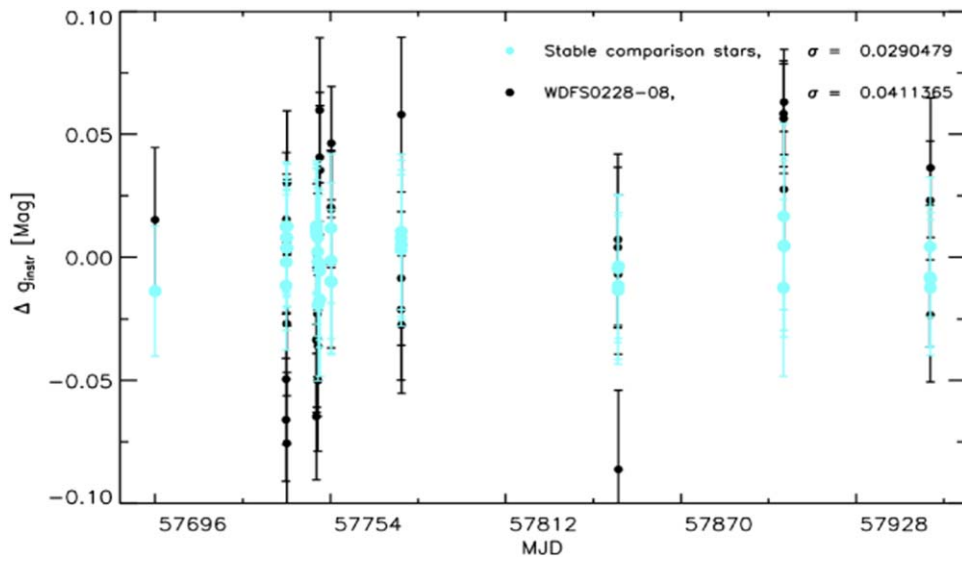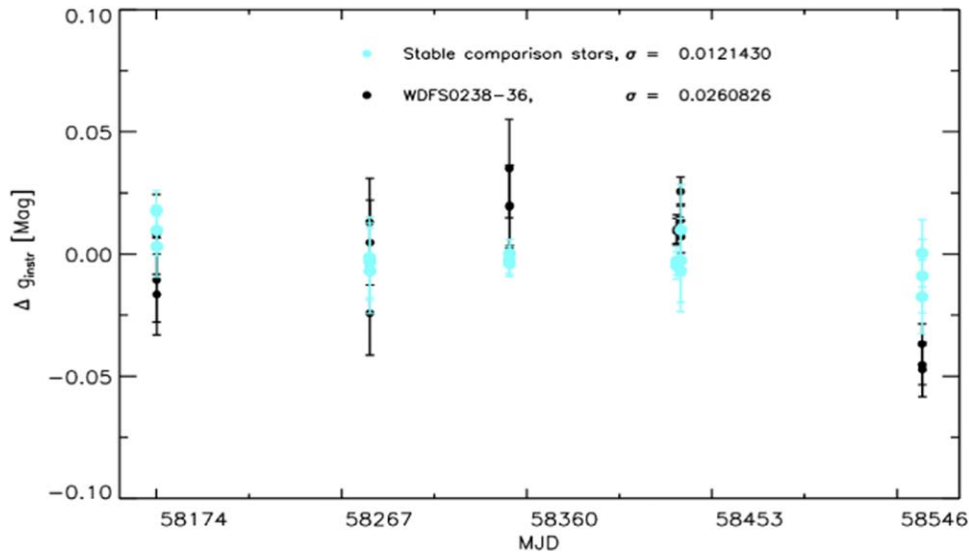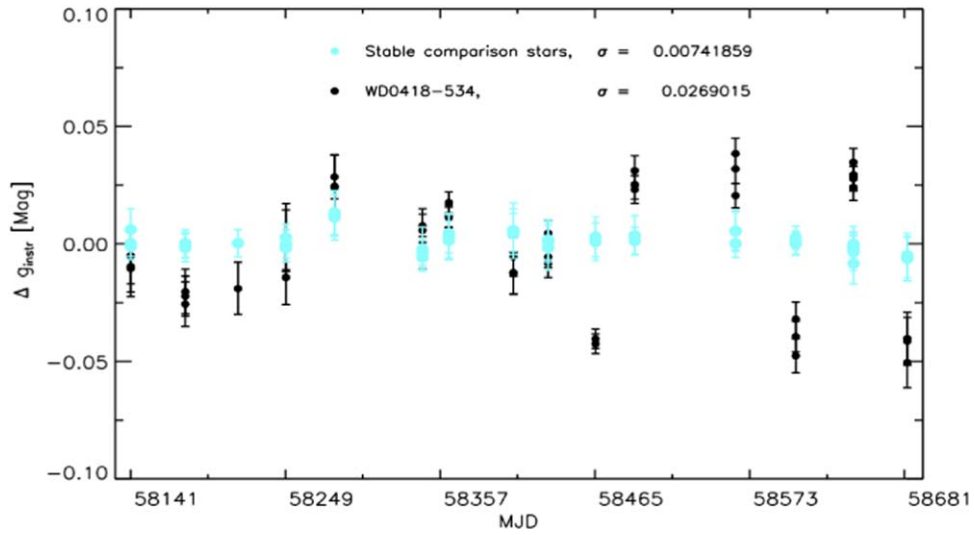

Figure 13. Same as Figure 12 but for star WDFS0228-08.
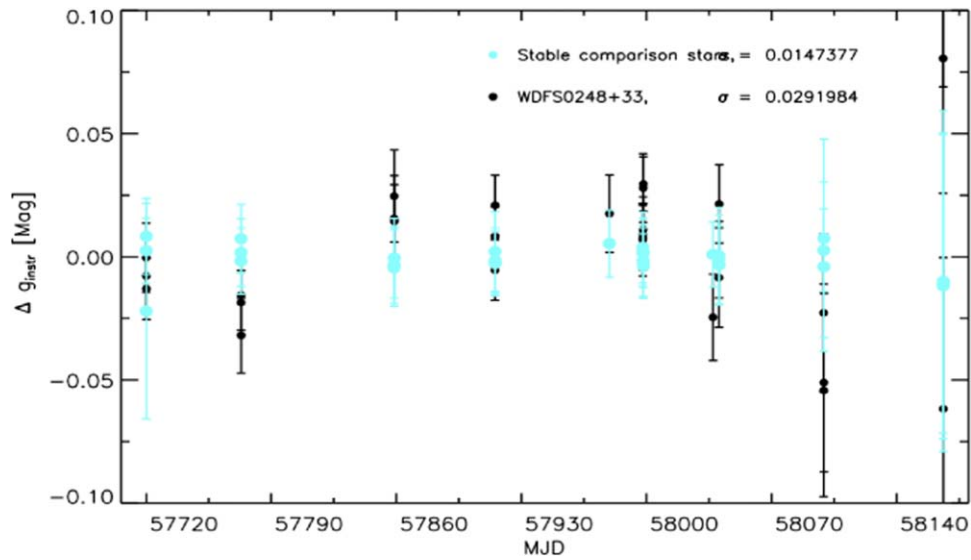
Figure 14. Same as Figure 12 but for star WDFS0248+33.
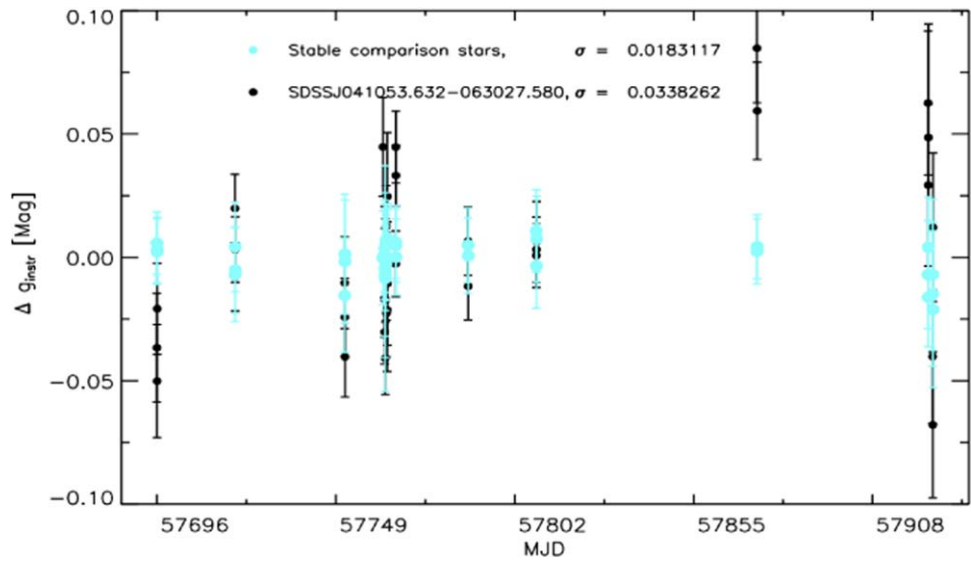
Figure 15. Same as Figure 12 but for star SDSSJ041053.632-063027.580.
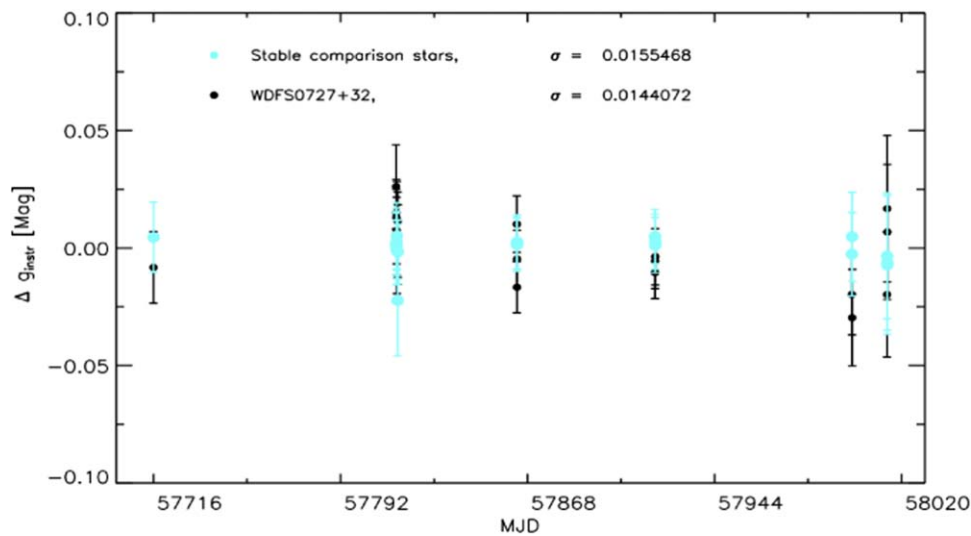
Figure 16. Same as Figure 12 but for star WDFS0727+32.
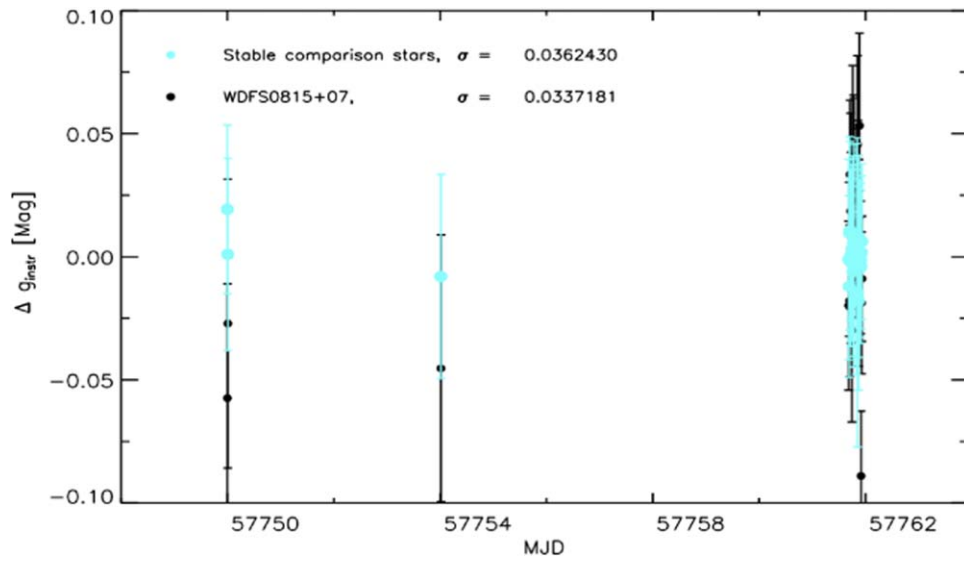
Figure 17. Same as Figure 12 but for star WDFS0815+07.
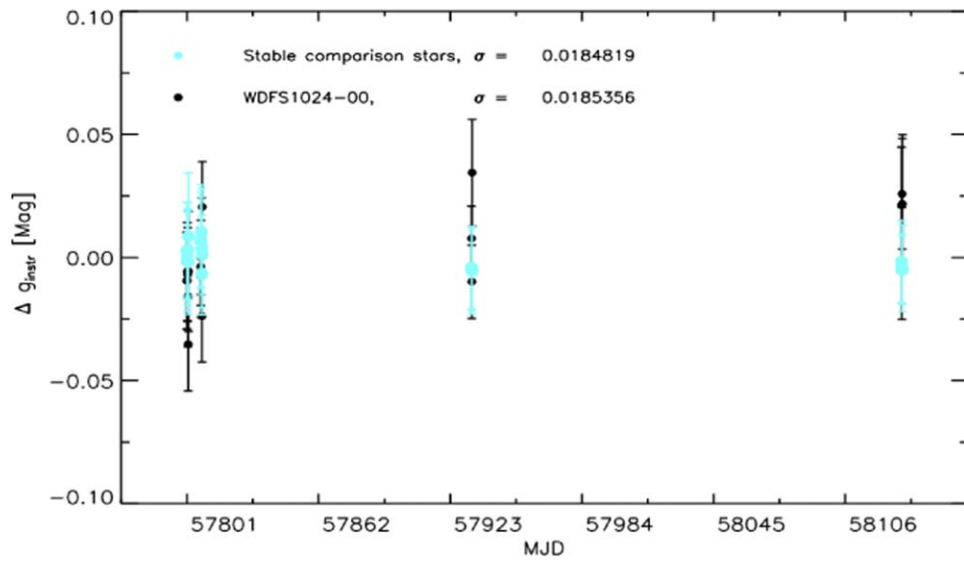
Figure 18. Same as Figure 12 but for star WDFS1024-00.
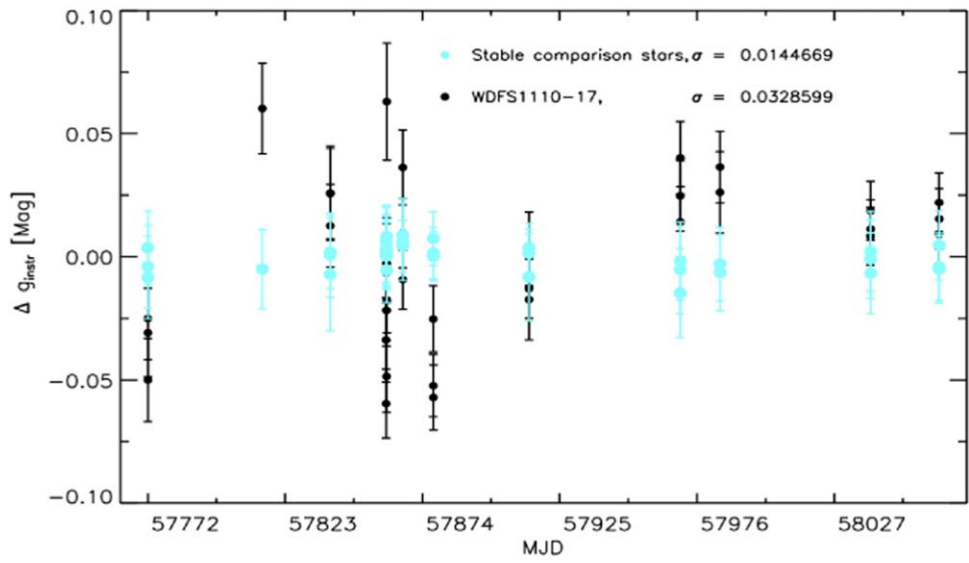
Figure 19. Same as Figure 12 but for star WDFS1110-17.
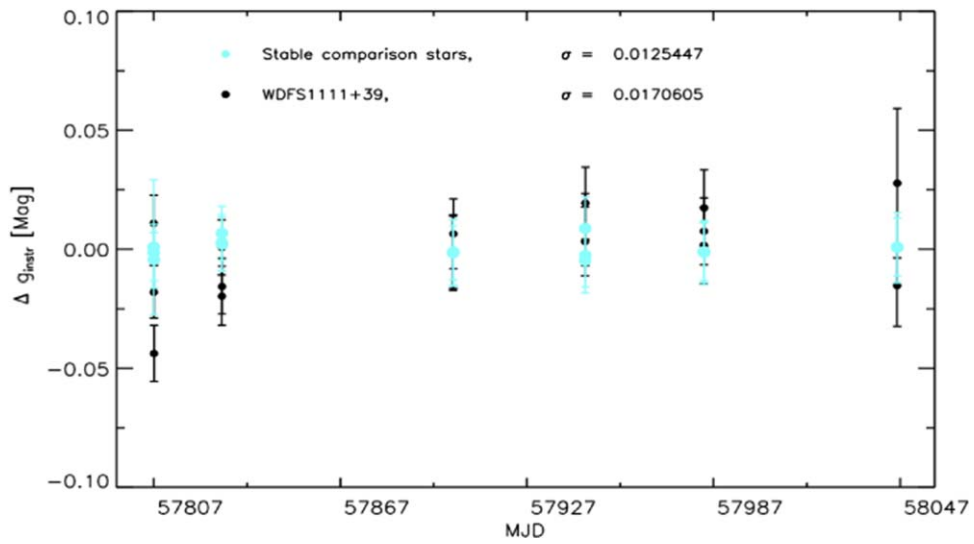
Figure 20. Same as Figure 12 but for star WDFS1111+39.
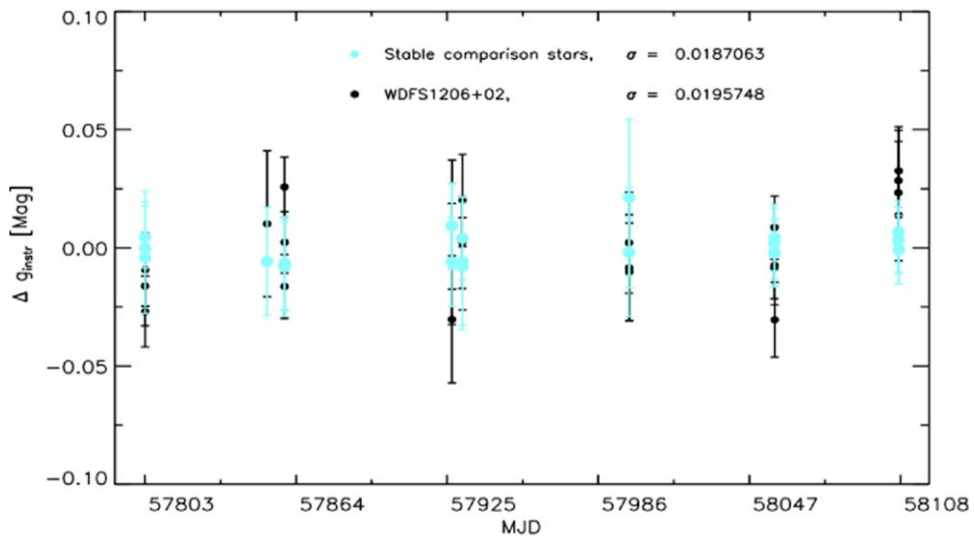
Figure 21. Same as Figure 12 but for star WDFS1206+02.
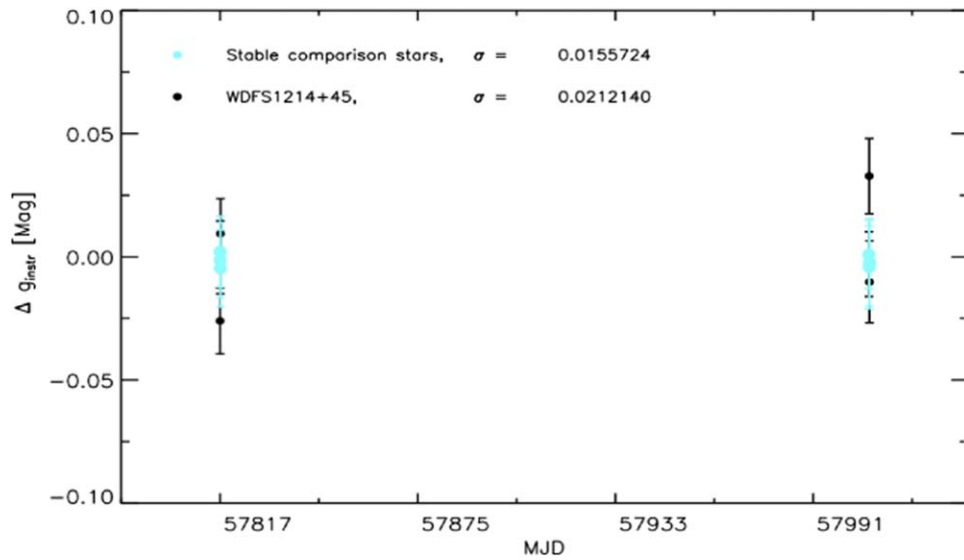
Figure 22. Same as Figure 12 but for star WDFS1214+45.
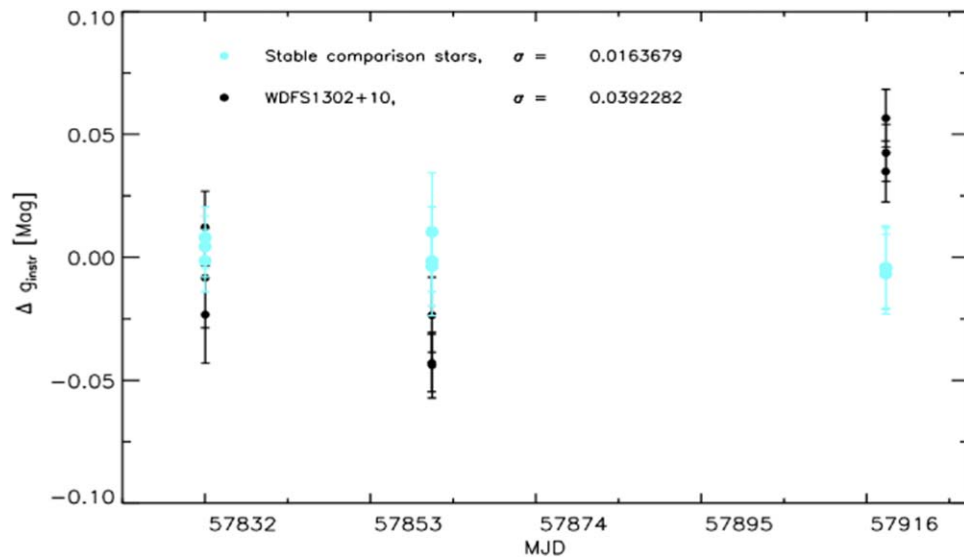
Figure 23. Same as Figure 12 but for star WDFS1302+10.
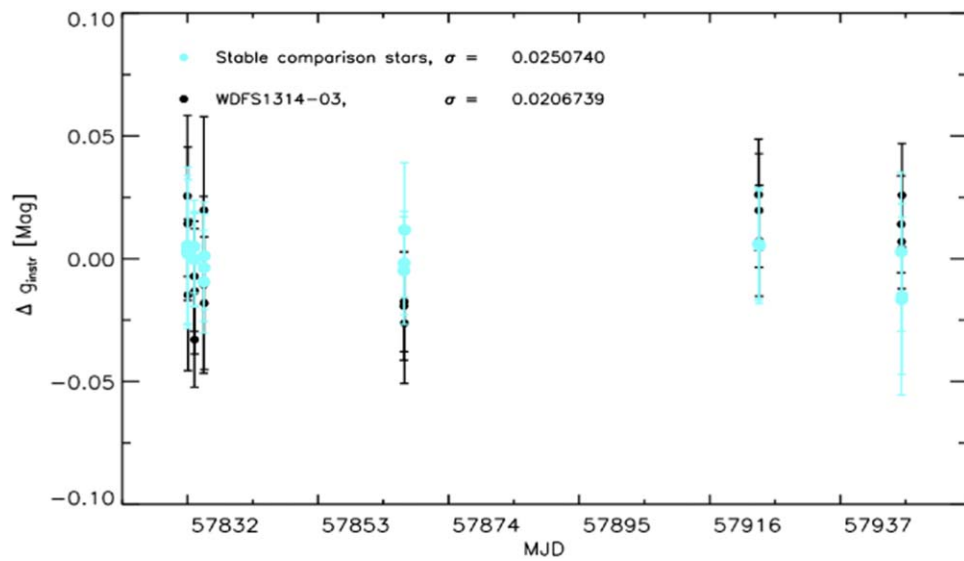
Figure 24. Same as Figure 12 but for star WDFS1314-03.
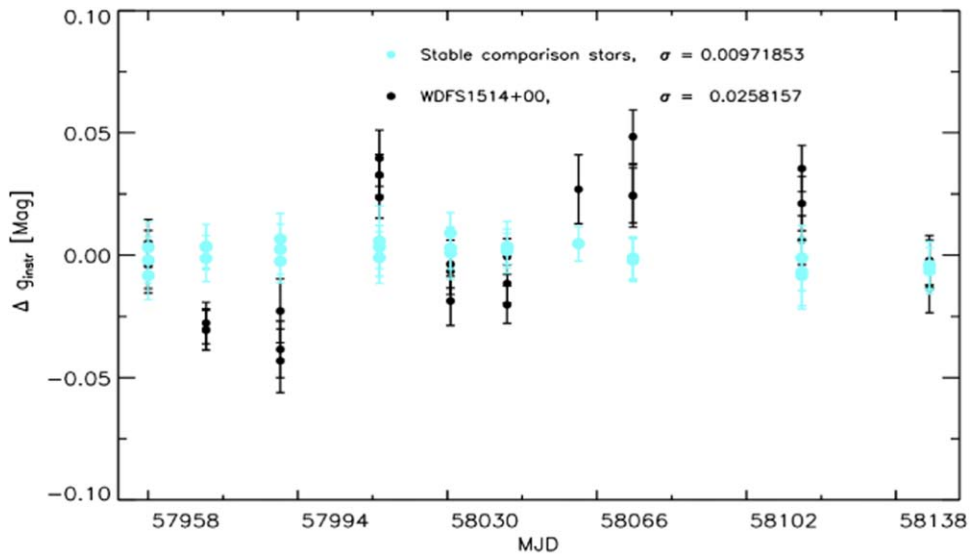
Figure 25. Same as Figure 12 but for star WDFS1514+00.
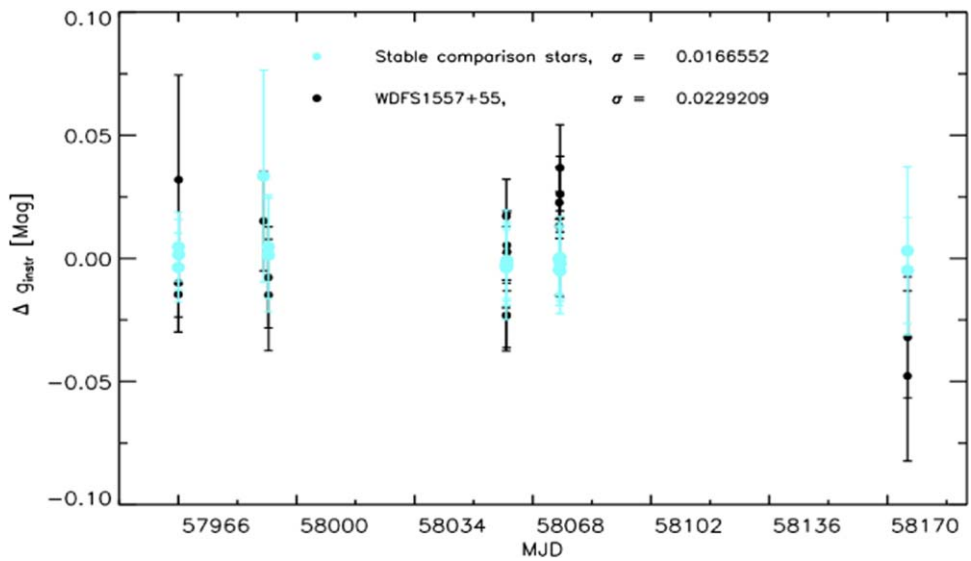
Figure 26. Same as Figure 12 but for star WDFS1557+55.
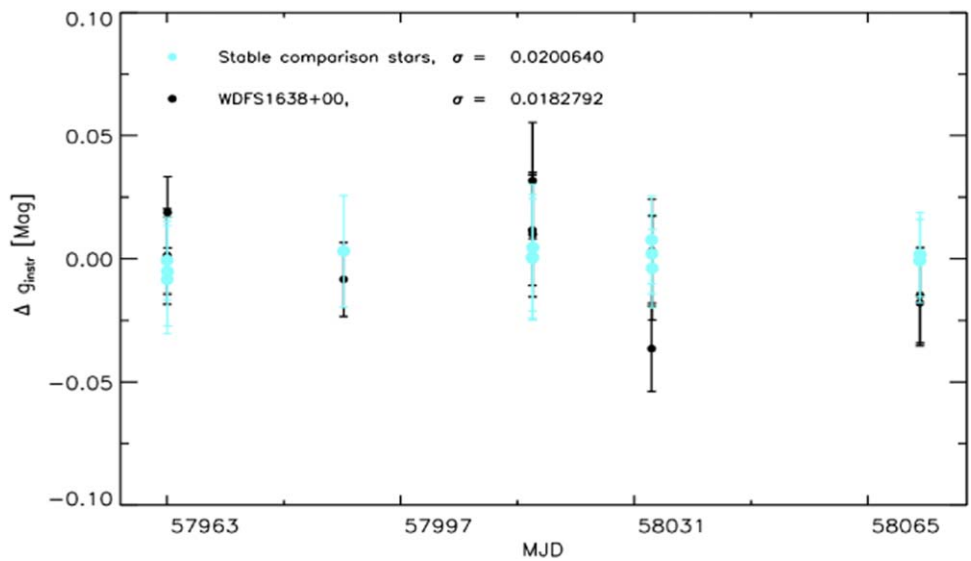
Figure 27. Same as Figure 12 but for star WDFS1638+00.
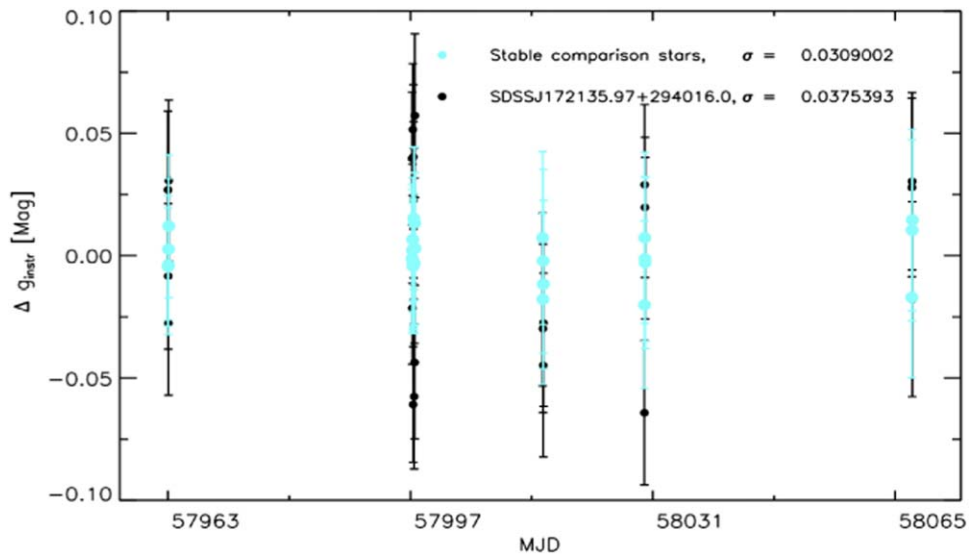
Figure 28. Same as Figure 12 but for star SDSSJ172135.97+294016.0.
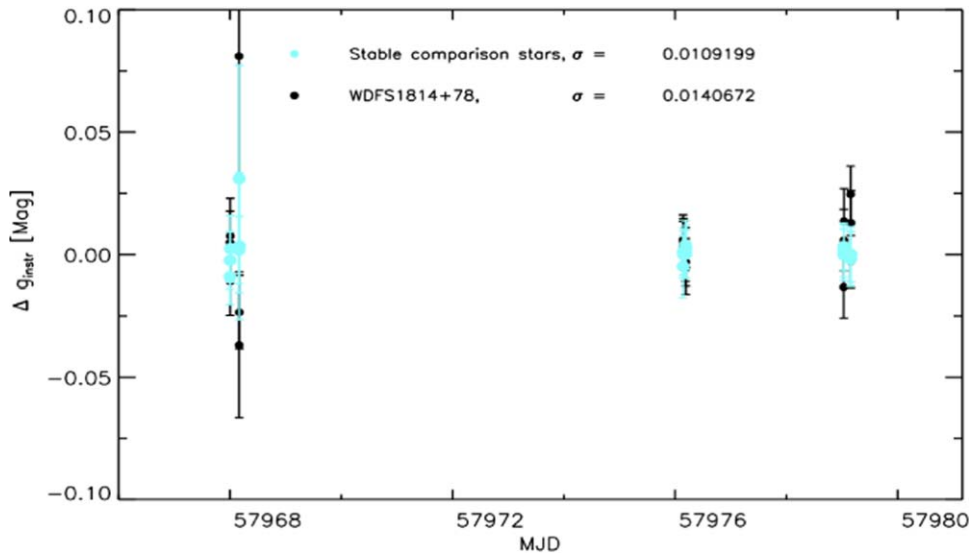
Figure 29. Same as Figure 12 but for star WDFS1814+78.
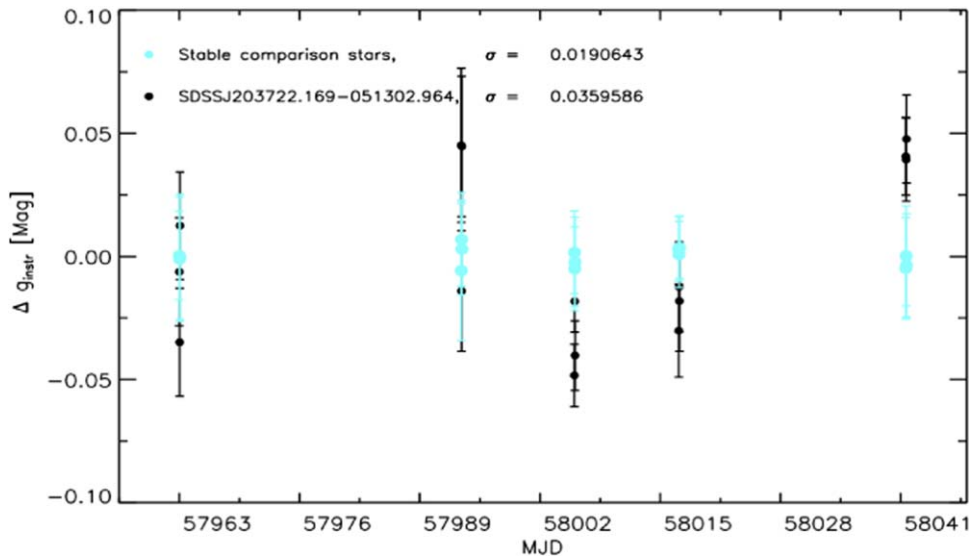
Figure 30. Same as Figure 12 but for star SDSSJ203722.169-051302.964.
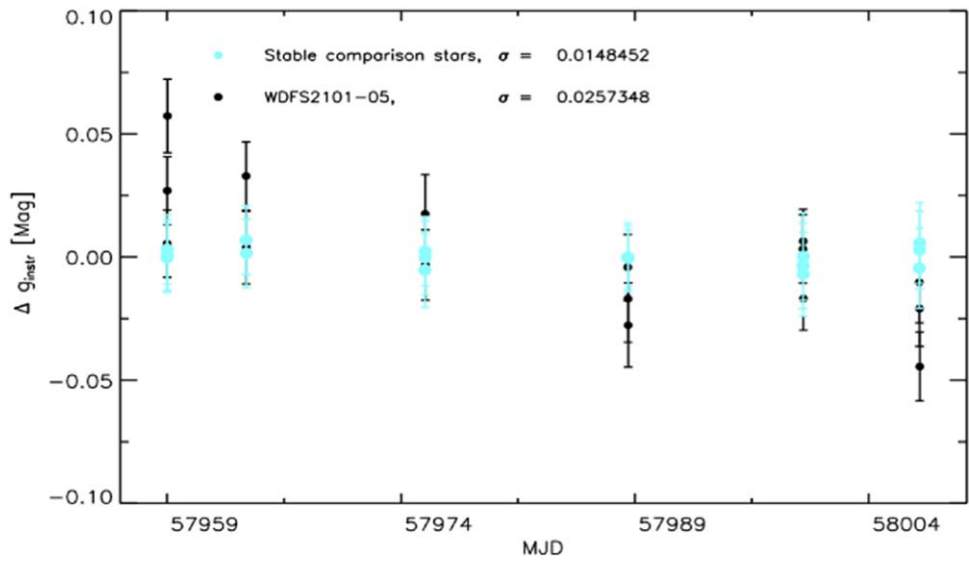
Figure 31. Same as Figure 12 but for star WDFS2101-05.
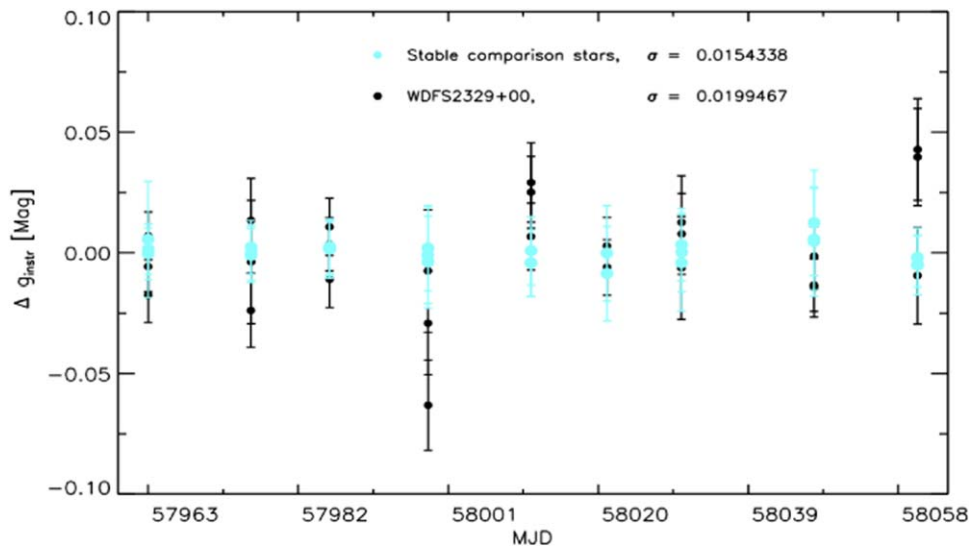
Figure 32. Same as Figure 12 but for star WDFS2329+00.

Appendix B
Southern DAWD Light Curves

The light curves for all the 15 DAWDs in the Southern hemisphere are shown in Figures 33–47. Plots are listed in order of increasing R.A.

Figure 33. Single epoch minus the mean instrumental magnitude measurements for WDFS0122-30 as a function of observing epoch (black crosses). Averaged and binned relative magnitudes for a set of stable stars of comparable instrumental magnitude in the same FoV are overplotted as a red-shaded area. The variability index of the selected stars and the measurement dispersion are listed. Error bars are shown.

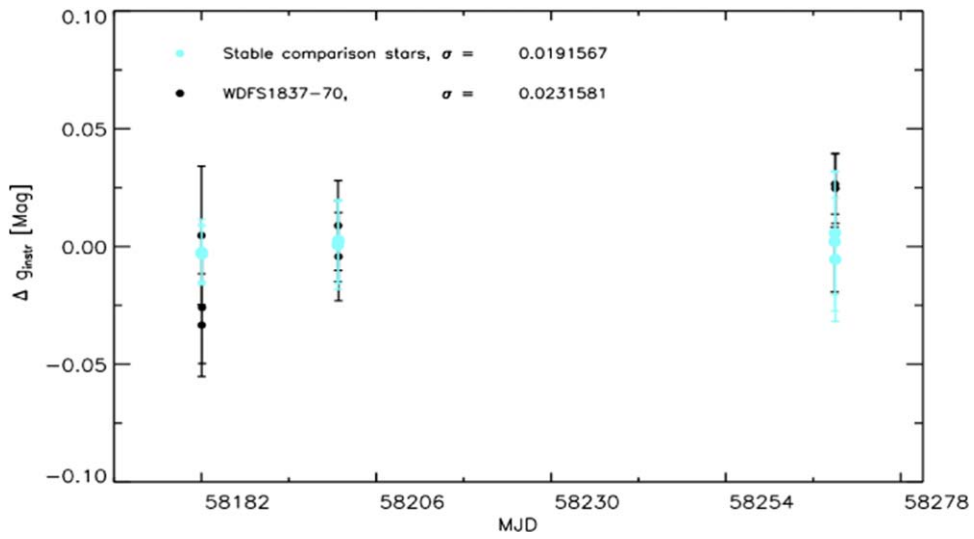**Figure 34.** Same as Figure 33 but for star WDFS0238-36.

Figure 35. Same as Figure 33 but for star WD0418-534.
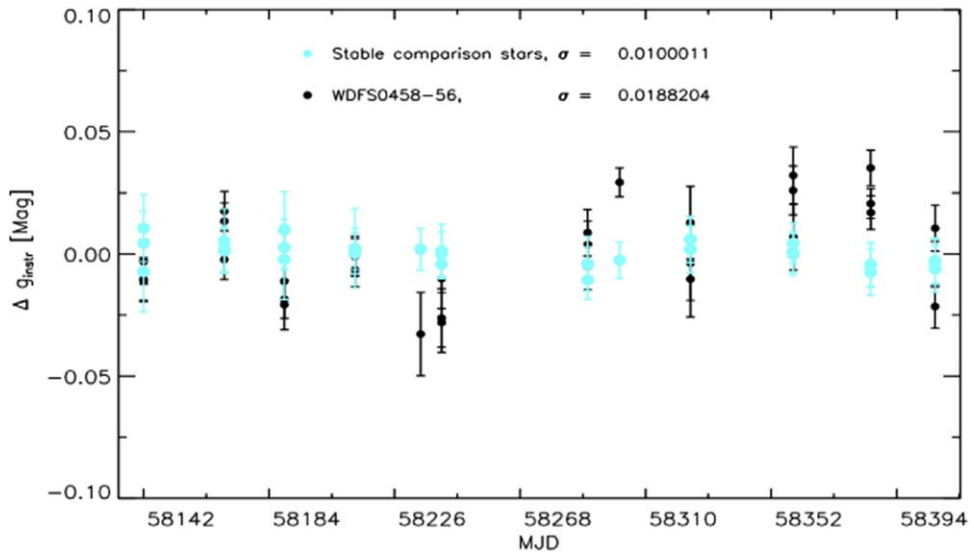
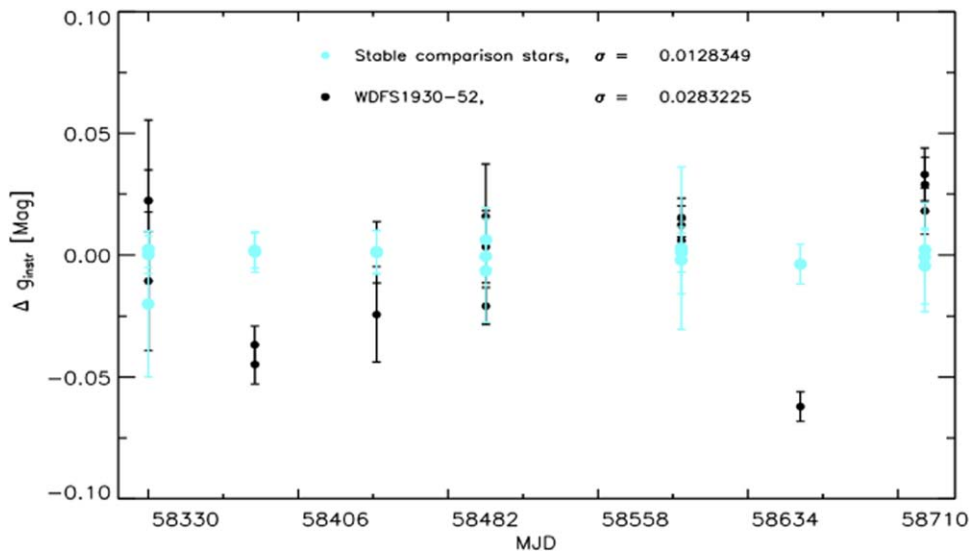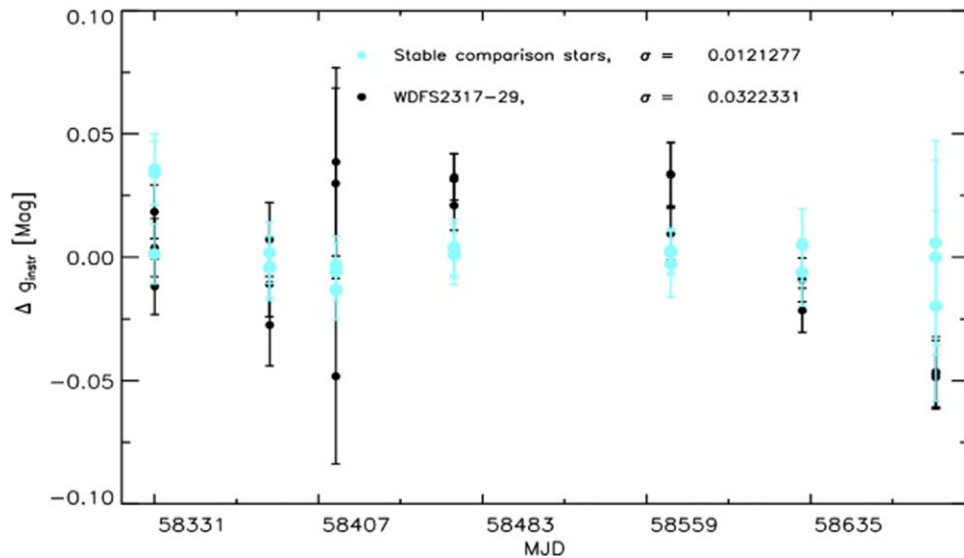**Figure 36.** Same as Figure 33 but for star WDFS0458-56.
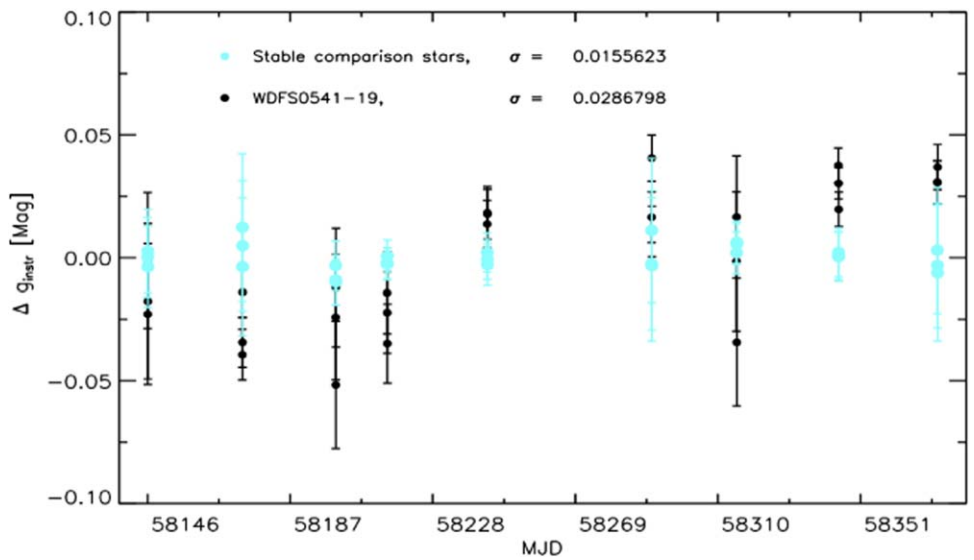
Figure 37. Same as Figure 33 but for star WDFS0541-19.
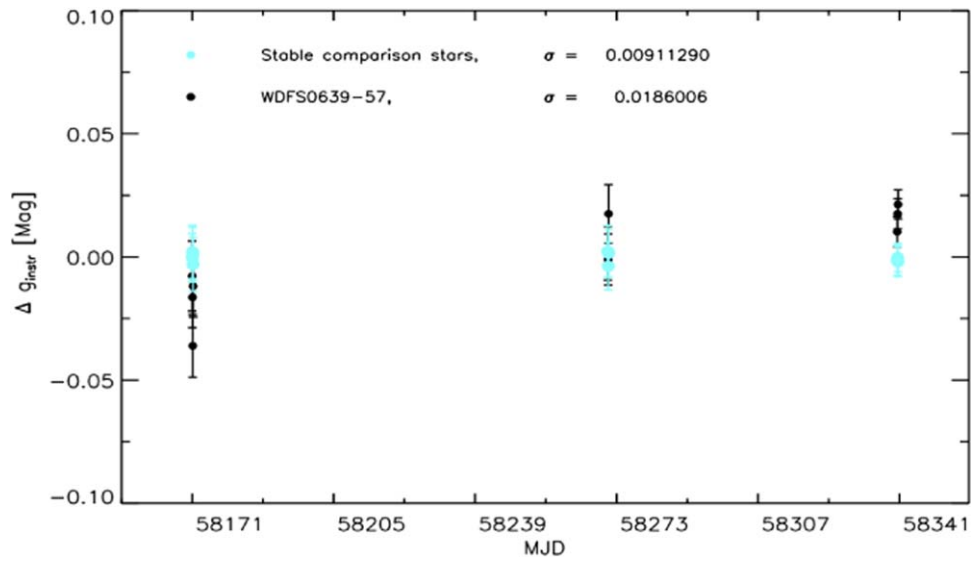
Figure 38. Same as Figure 33 but for star WDFS0639-57.
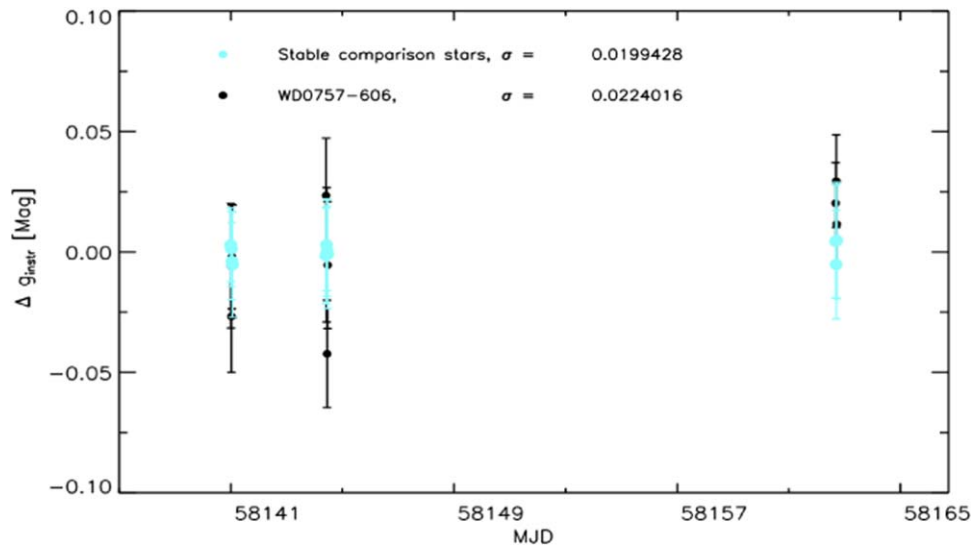
Figure 39. Same as Figure 33 but for star WD0757-606.
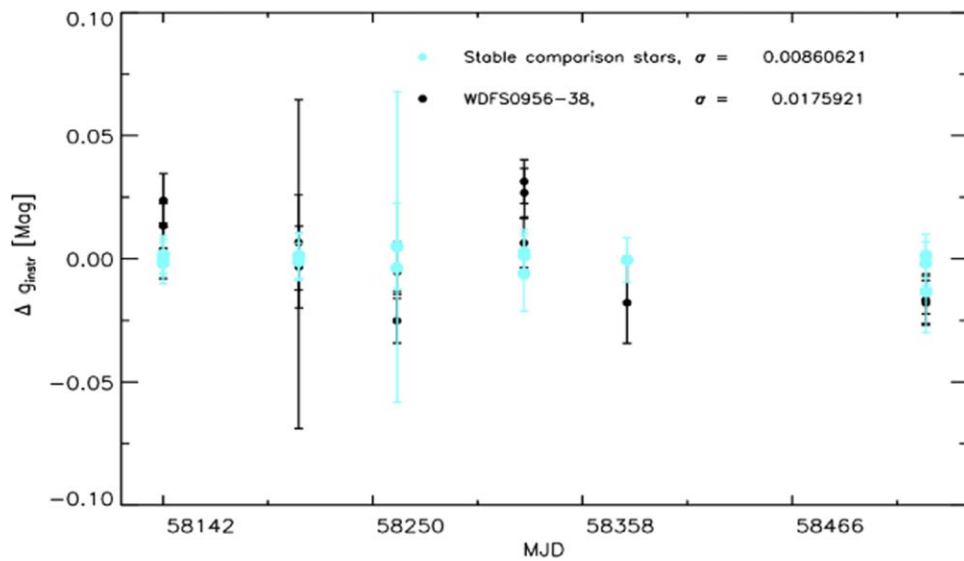
Figure 40. Same as Figure 33 but for star WDFS0956-38.
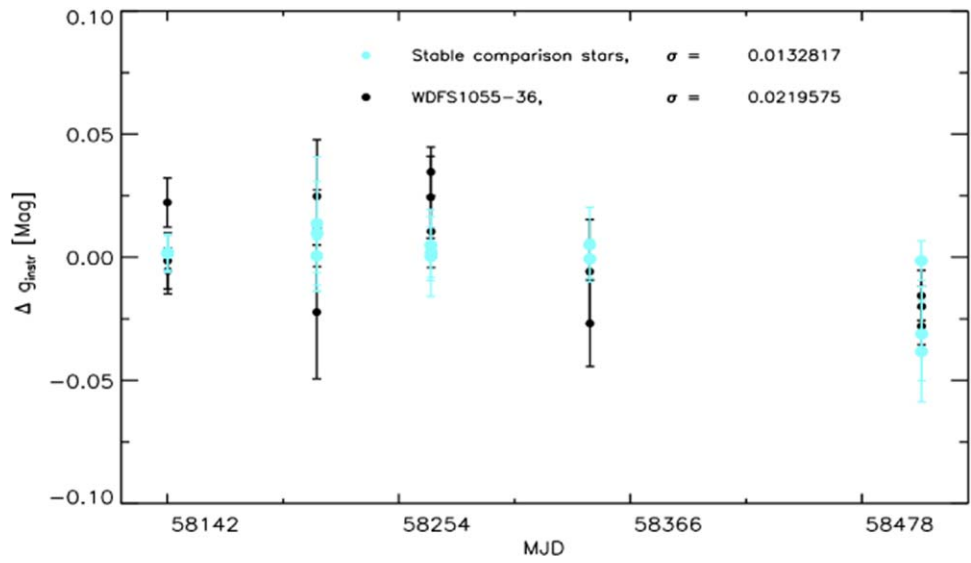
Figure 41. Same as Figure 33 but for star WDFS1055-36.
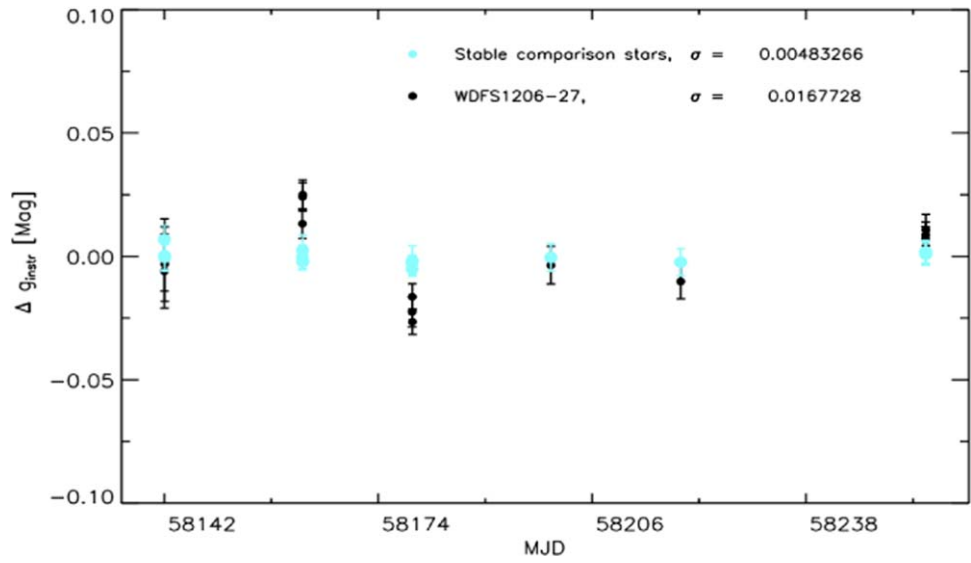
Figure 42. Same as Figure 33 but for star WDFS1206-27.
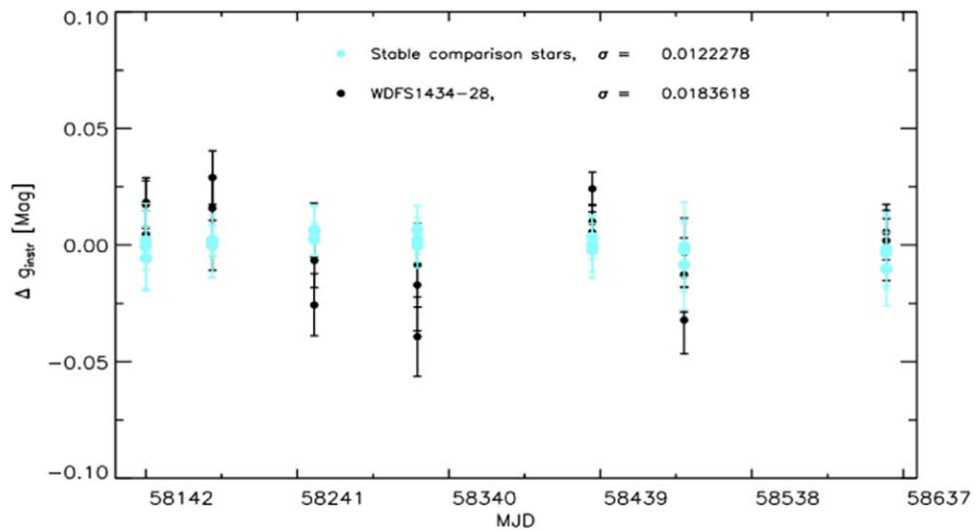
Figure 43. Same as Figure 33 but for star WDFS1434-28.
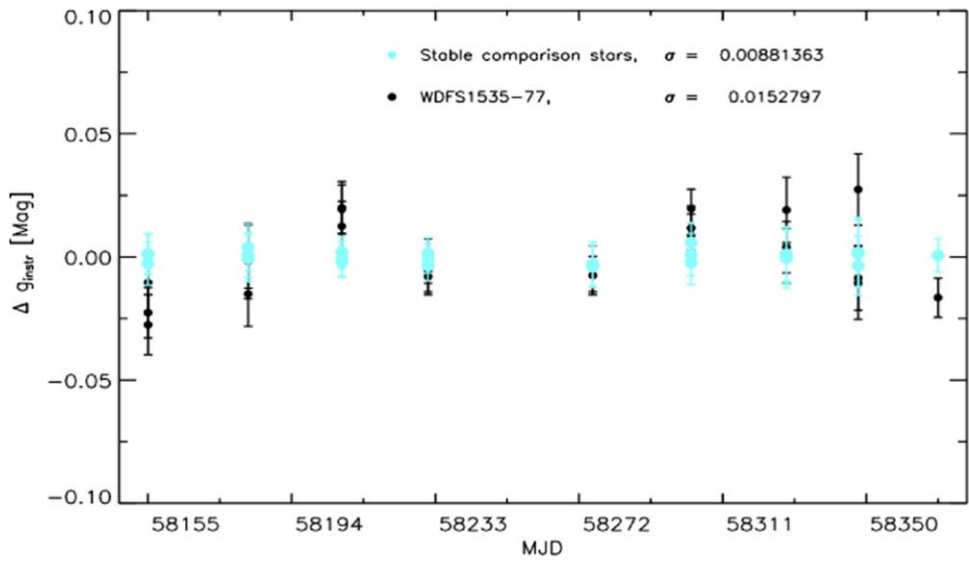
Figure 44. Same as Figure 33 but for star WDFS1535-77.

Figure 45. Same as Figure 33 but for star WDFS1837-70.

Figure 46. Same as Figure 33 but for star WDFS1930-52.

Figure 47. Same as Figure 33 but for star WDFS2317-29.

Appendix C
Finding Charts

We provide here finding charts for the 23 Northern and the 15 Southern DAWDs (Figures 48–50). These are based on *drizzled* WFC3/HST images collected in the F160W filter and cover an FoV of $26'' \times 26''$. Some background objects and faint red dwarfs are visible in the NIR but are absent in the bluer WFC3/HST filter images and the LCO g-band images. In particular, due to the larger pixel scale ($\approx 0.''39$ versus $0.''13$ pixel^{-1}) and to the seeing, these faint red objects, which could be as close as $\lesssim 0.''5$–$2''$ to the DAWDs, might contaminate the LCO light curves. These contaminants are difficult or impossible to separate and identify on the LCO g-band images. Thus, we provide the following higher-resolution NIR finding charts. In addition, we warn observers using ground-based facilities to be aware of potential NIR contamination for some of the DAWDs selected as standards. For more details see the discussion in Section 5 and Table 4.
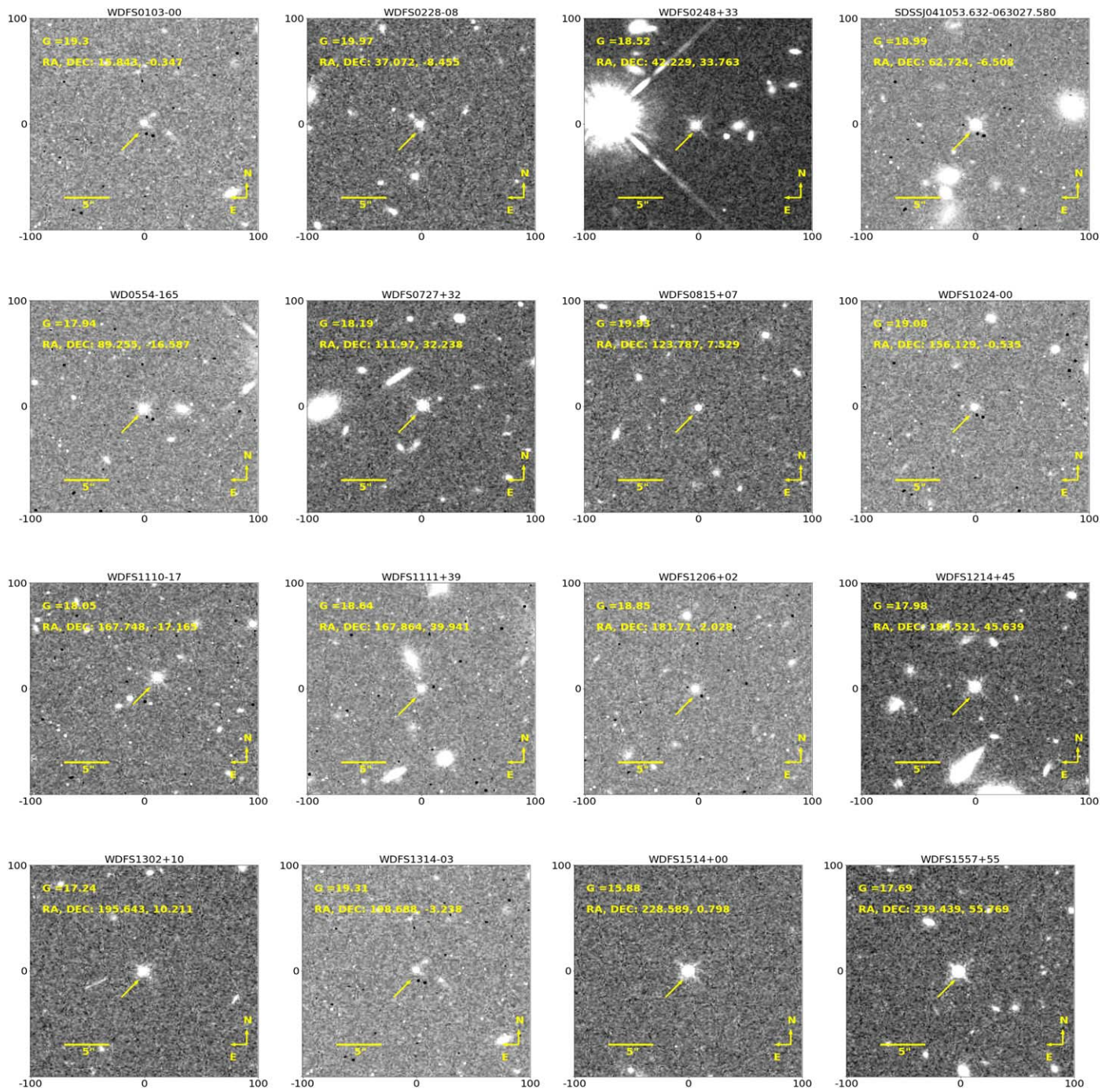
Figure 48. Finding charts for 16 candidate DAWDs based on WFC3 drizzled F160W image cutouts centered on the star and covering an FoV of $26'' \times 26''$. Star Gaia DR3 magnitude and coordinates are labeled on the image. The yellow solid arrow points at the DAWD and the yellow line indicates $5''$ on the image. The North and East directions are also shown.
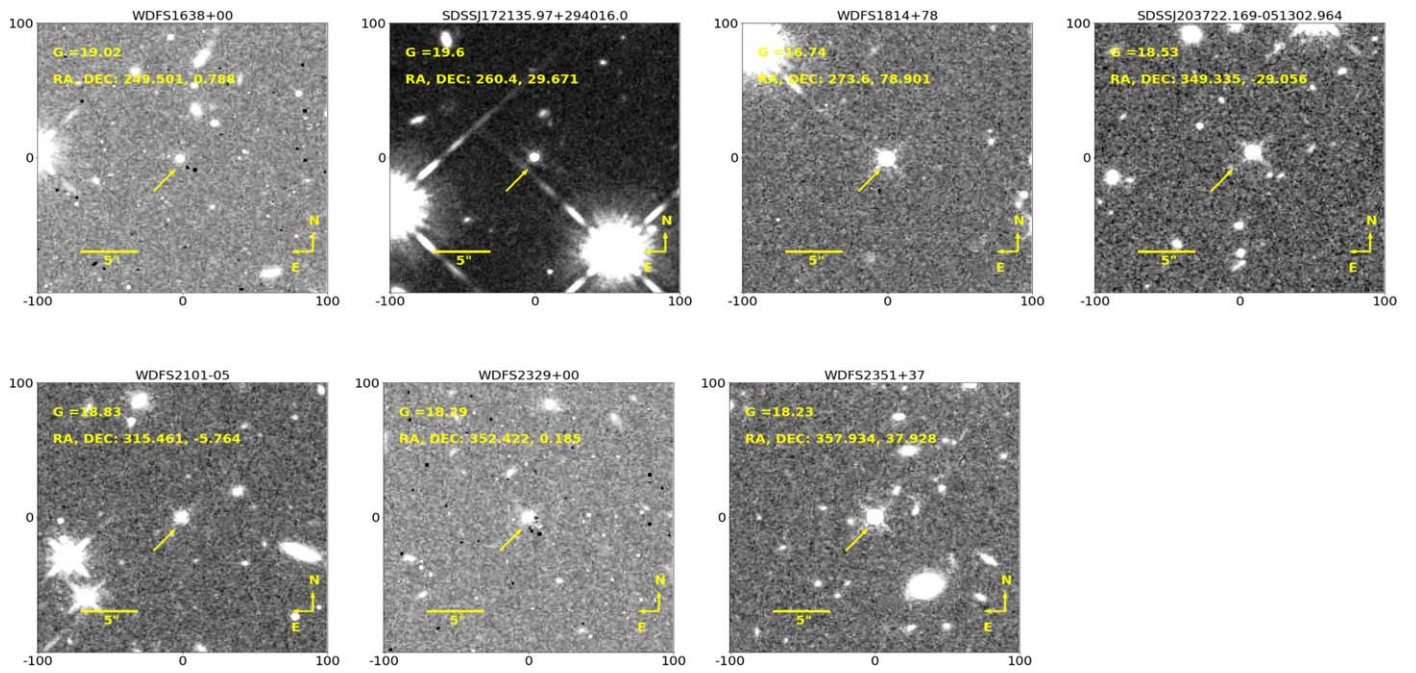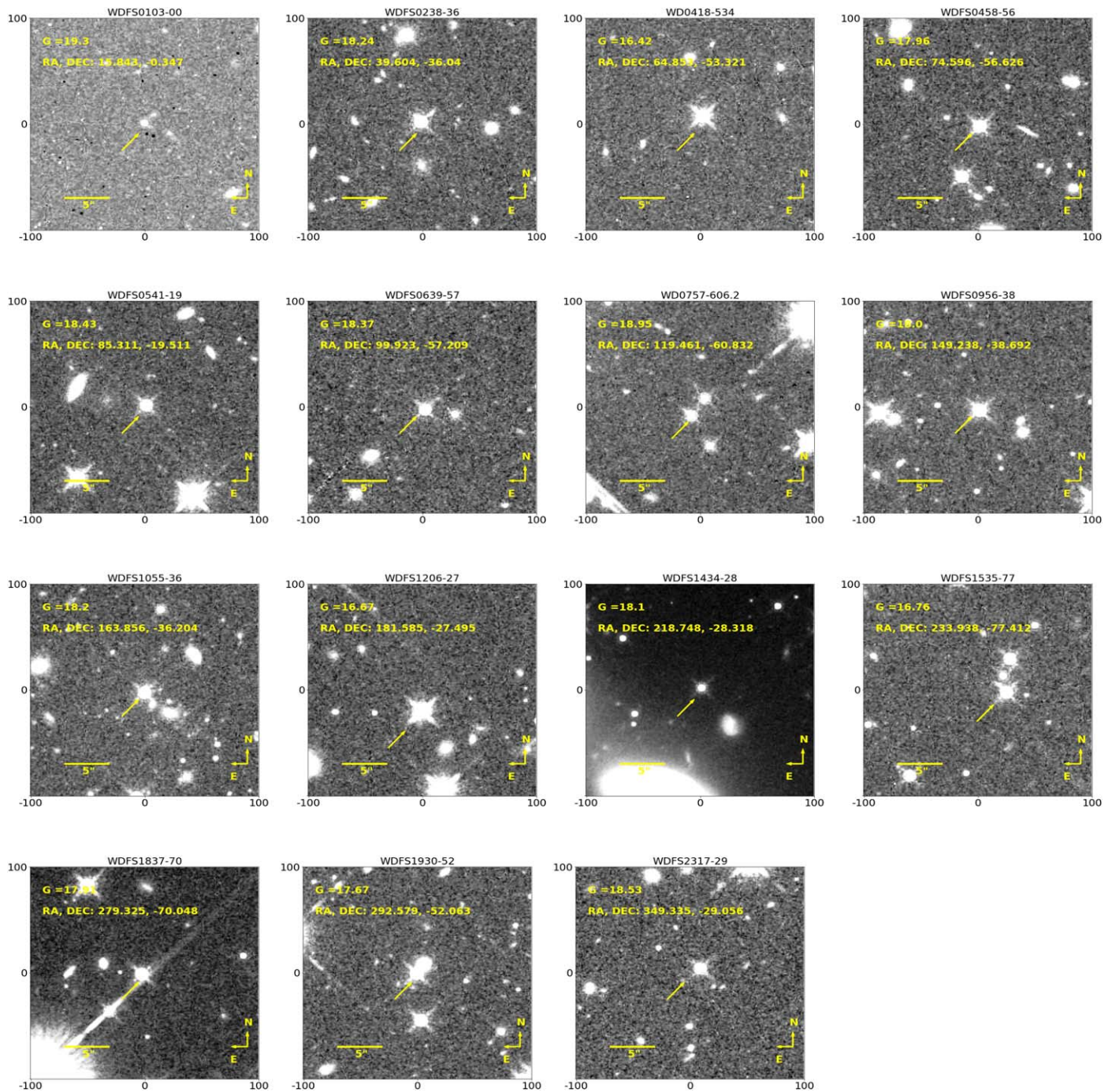
Figure 49. Finding charts for 7 candidate DAWDs based on WFC3 drizzled F160W image cutouts centered on the star and covering an FoV of $26'' \times 26''$. Star Gaia DR3 magnitude and coordinates are labeled on the image. The yellow solid arrow points at the DAWD and the yellow line indicates $5''$ on the image. The north and east directions are also shown.

Figure 50. Finding charts for 15 candidate DAWDs based on WFC3 drizzled F160W image cutouts centered on the star and covering an FoV of $26'' \times 26''$. Star Gaia DR3 magnitude and coordinates are labeled on the image. The yellow solid arrow points at the DAWD and the yellow line indicates $5''$ on the image. The north and east directions are also shown.

ORCID iDs

Annalisa Calamida ⓘ https://orcid.org/0000-0002-0882-7702
Thomas Matheson ⓘ https://orcid.org/0000-0001-6685-0479
Edward W. Olszewski ⓘ https://orcid.org/0000-0002-7157-500X
Abhijit Saha ⓘ https://orcid.org/0000-0002-6839-4881
Tim Axelrod ⓘ https://orcid.org/0000-0002-5722-7199
Sean Points ⓘ https://orcid.org/0000-0002-4596-1337
Gautham Narayan ⓘ https://orcid.org/0000-0001-6022-0484

Konstantin Malanchev ⓘ https://orcid.org/0000-0001-7179-7406
Ryan Ridden-Harper ⓘ https://orcid.org/0000-0003-1724-2885
Nicola Gentile-Fusillo ⓘ https://orcid.org/0000-0002-6428-4378
Roberto Raddi ⓘ https://orcid.org/0000-0002-9090-9191
Ralph Bohlin ⓘ https://orcid.org/0000-0001-9806-0551
Armin Rest ⓘ https://orcid.org/0000-0002-4410-5387
Ivan Hubeny ⓘ https://orcid.org/0000-0001-8816-236X

Susana Deustua ⬤ https://orcid.org/0000-0003-2823-360X
Elena Sabbi ⬤ https://orcid.org/0000-0003-2954-7643
Christopher W. Stubbs ⬤ https://orcid.org/0000-0003-0347-1724

References

Adelman-McCarthy, J. K., Agüeros, M. A., Allam, S. S., et al. 2008, ApJS, 175, 297

Bayo, A., Rodrigo, C., Barrado Y Navascués, D., et al. 2008, A&A, 492, 277

Bellm, E. C., Kulkarni, S. R., Graham, M. J., et al. 2019, PASP, 131, 018002

Bertin, E., & Arnouts, S. 1996, A&AS, 117, 393

Betoule, M., Kessler, R., Guy, J., et al. 2014, A&A, 568, A22

Bohlin, R. C. 2014, AJ, 147, 127

Bohlin, R. C., Hubeny, I., & Rauch, T. 2020, AJ, 160, 21

Brinkworth, C. S., Burleigh, M. R., Lawrie, K., Marsh, T. R., & Knigge, C. 2013, ApJ, 773, 47

Brinkworth, C. S., Burleigh, M. R., Wynn, G. A., & Marsh, T. R. 2004, MNRAS, 348, L33

Brout, D., Taylor, G., Scolnic, D., et al. 2022, ApJ, 938, 111

Calamida, A., Matheson, T., Saha, A., et al. 2019, ApJ, 872, 199

Chu, Y.-H., Guerrero, M. A., Gruendl, R. A., & Webbink, R. F. 2004, AJ, 127, 477

Clemens, J. C., Crain, J. A., & Anderson, R. 2004, Proc. SPIE, 5492, 331

Dupuis, J., Chayer, P., Vennes, S., Christian, D. J., & Kruk, J. W. 2000, ApJ, 537, 977

Fontaine, G., & Brassard, P. 2008, PASP, 120, 1043

Gentile Fusillo, N. P., Raddi, R., Gänsicke, B. T., et al. 2017, MNRAS, 469, 621

Gaia Collaboration, Vallenari, A., Brown, A. G. A., et al. 2022, arXiv:2208.00211

Girven, J., Steeghs, D., Heber, U., et al. 2012, MNRAS, 425, 1013

Gorecki, A., Abate, A., Ansari, R., et al. 2014, A&A, 561, A128

Heinze, A. N., Tonry, J. L., Denneau, L., et al. 2018, AJ, 156, 241

Hermes, J. J., Gänsicke, B. T., Gentile Fusillo, N. P., et al. 2017, MNRAS, 468, 1946

Holberg, J. B., & Howell, S. B. 2011, AJ, 142, 62

Hook, I. M., Jørgensen, I., Allington-Smith, J. R., et al. 2004, PASP, 116, 425

Kleinman, S. J., Kepler, S. O., Koester, D., et al. 2013, ApJS, 204, 5

Magnier, E. A., Sweeney, W. E., Chambers, K. C., et al. 2020, ApJS, 251, 5

Malanchev, K. L., Pruzhinskaya, M. V., Korolev, V. S., et al. 2021, MNRAS, 502, 5147

McCook, G. P., & Sion, E. M. 1999, ApJS, 121, 1

Narayan, G., Matheson, T., Saha, A., et al. 2019, ApJS, 241, 20

Qi, Z., Yu, Y., Bucciarelli, B., et al. 2015, AJ, 150, 137

Raddi, R., Catalán, S., Gänsicke, B. T., et al. 2016, MNRAS, 457, 1988

Raddi, R., Gentile Fusillo, N. P., Pala, A. F., et al. 2017, MNRAS, 472, 4173

Ridden-Harper, R., Rest, A., Hounsell, R., et al. 2021, arXiv:2111.15006

Saha, A., Vivas, A. K., Olszewski, E. W., et al. 2019, ApJ, 874, 30

Schechter, P. L., Mateo, M., & Saha, A. 1993, PASP, 105, 1342

Scolnic, D., Brout, D., Carr, A., et al. 2022, ApJ, 938, 113

Scolnic, D., Casertano, S., Riess, A., et al. 2015, ApJ, 815, 117

Scolnic, D., Perlmutter, S., Aldering, G., et al. 2019, Astro2020: Decadal Survey on Astronomy and Astrophysics, National Academies, 270

Sokolovsky, K. V., Gavras, P., Karampelas, A., et al. 2017, MNRAS, 464, 274

Stetson, P. B. 1987, PASP, 99, 191

Stetson, P. B. 1994, PASP, 106, 250

Stubbs, C. W., & Brown, Y. J. 2015, MPLA, 30, 1530030

Tonry, J. L., Denneau, L., Heinze, A. N., et al. 2018, PASP, 130, 064505

Toonen, S., Hollands, M., Gänsicke, B. T., & Boekholt, T. 2017, A&A, 602, A16